Molecular Imaging of Hypoxia

Kenneth A. Krohn[1], Jeanne M. Link[1], and Ralph P. Mason[2]

[1]*Department of Radiology, University of Washington, Seattle, Washington; and* [2]*Department of Radiology, University of Texas, Southwestern Medical Center, Dallas, Texas*

Hypoxia, a condition of insufficient O_2 to support metabolism, occurs when the vascular supply is interrupted, as in stroke or myocardial infarction, or when a tumor outgrows its vascular supply. When otherwise healthy tissues lose their O_2 supply acutely, the cells usually die, whereas when cells gradually become hypoxic, they adapt by up-regulating the production of numerous proteins that promote their survival. These proteins slow the rate of growth, switch the mitochondria to glycolysis, stimulate growth of new vasculature, inhibit apoptosis, and promote metastatic spread. The consequence of these changes is that patients with hypoxic tumors invariably experience poor outcome to treatment. This has led the molecular imaging community to develop assays for hypoxia in patients, including regional measurements from O_2 electrodes placed under CT guidance, several nuclear medicine approaches with imaging agents that accumulate with an inverse relationship to O_2, MRI methods that measure either oxygenation directly or lactate production as a consequence of hypoxia, and optical methods with NIR and bioluminescence. The advantages and disadvantages of these approaches are reviewed, along with the individual strategies for validating different imaging methods. Ultimately the proof of value is in the clinical performance to predict outcome, select an appropriate cohort of patients to benefit from a hypoxia-directed treatment, or plan radiation fields that result in better local control. Hypoxia imaging in support of molecular medicine has become an important success story over the last decade and provides a model and some important lessons for development of new molecular imaging probes or techniques.

Key Words: hypoxia; ^{18}F-FMISO; Cu-ATSM; biomarkers; bioluminescence; MRI

J Nucl Med 2008; 49:129S–148S
DOI: 10.2967/jnumed.107.045914

Oxygen is an essential nutrient for mammalian cells because of its role as the terminal electron acceptor in oxidative phosphorylation. Supplied through breathing, O_2 dissolves in plasma and tissues and is carried throughout the body as oxyhemoglobin, O_2Hb, which releases O_2 when it is needed for mitochondrial respiration. It is so essential to the well-being of cells that intricate control mechanisms have evolved to maintain a sufficient supply of O_2 for the mitochondria. This control system can adjust blood flow, blood vessel dilation, or oxygen extraction fraction to maintain a life-sustaining level of O_2.

In the brain, oxygen physiology changes rapidly in response to stimulation by simple tasks such as visual or auditory input or language function, and this rapid response is monitored in functional mapping of the brain using PET (*1*) or fMRI (*1,2*). These processes also change in response to stroke and have been studied with a protocol using ^{15}O-O_2 plus its metabolite, ^{15}O-H_2O, and the measurement of vascular volume using inhaled ^{15}O or ^{11}C-labeled CO, which binds to red cells as COHb (*3,4*). A qualitative version of this test has been used to select appropriate subjects for the carotid occlusion surgical study (*5,6*).

When otherwise healthy cells are suddenly deprived of sufficient O_2 to maintain oxidative phosphorylation, the cells die either by necrosis or programmed cell death, apoptosis. This phenomenon is called hypoxia and it happens, for example, in stroke, myocardial infarction, or as a consequence of poor perfusion in diabetic limbs or arthritic joints. Cancer cells often respond to hypoxia in a different way, as will be discussed in the next section.

Hypoxia is therefore a phenomenologic concept. There is no specific value of O_2Hb concentration, % Hb saturation by oximetry, or tissue partial pressure, PO_2 measured with electrodes, that results in a transition from normoxia to hypoxia. Of course, PO_2 gradients also exist from the point of supply (vasculature) to consumption (mitochondria). The biologic consequences of hypoxia depend on duration and the needs of individual cells; speed is critical in reestablishing perfusion after a stroke or infarction.

Clearly, the ability to identify hypoxia has implications in a wide range of medical settings. How can this best be accomplished? The goal is to develop a positive image of the absence of something, namely O_2, because the critical effect happens when O_2 levels are too low to satisfy the metabolic demand. Oxygen-sensitive electrodes, when properly calibrated, can directly measure PO_2 in units of mm Hg (*7–10*), but the signal is very small in the range of cell-threatening hypoxia. This technique has the practical disadvantages of requiring CT or ultrasound-guided placement, and accessible tissue beds limit sampling, and it invades and damages tissues. There are fluorescent needle probes where the optical signal is quenched by O_2 so that

Received Oct. 26, 2007; revision accepted Mar. 11, 2008.
For correspondence or reprints contact: Kenneth A. Krohn, Department of Radiology, University of Washington, 1959 NE Pacific St., Room NW041, Box 356004, Seattle, WA 98195-6004.
E-mail: kkrohn@u.washington.edu

the signal increases as O_2 values fall (*11–13*). This resolves one limitation of electrodes, but it still requires accessible sites. Fluorescent techniques also have much lower oxygen consumption than do electrodes, which may be particularly crucial at low PO_2.

MRI provides a useful way to measure hypoxia. Absolute PO_2 can be measured on the basis of fluorocarbon reporter molecules. These may be introduced by direct intratumoral injection and they provide measurements consistent with electrodes (presumably interstitial PO_2). A major advantage over electrodes is that maps of regional PO_2 may be measured at 50–150 individual locations simultaneously. Moreover, once the reporter molecule has been introduced, sequential PO_2 maps may be generated to reveal changes in oxygenation with respect to interventions, such as hyperoxic gas breathing or vascular targeting agents (*14,15*). Because of a lack of human MRI systems with a ^{19}F MRI capability, ^{19}F oximetry measurements have not yet been attempted in patients.

Blood Oxygen Level Dependant (BOLD) MRI is an imaging technique that distinguishes paramagnetic deoxy-Hb from O_2Hb. Appropriate T2*-weighted imaging reveals changes in vascular oxygenation. A limitation is that it is also sensitive to changes in Hb concentration, which may result from alterations in vascular volume and flow as well as interconversion of oxy- and deoxy-hemoglobin. Therefore, this technique provides qualitative assessment of changes in oxygenation rather than quantitative measurements. This technique is widely used for functional brain mapping (*1,16,17*), where it is thought to primarily reflect changes in flow. It is starting to be applied to tumor studies. BOLD is particularly responsive to oxygen manipulation accompanying hyperoxic gas breathing as a simple way to ameliorate hypoxia (*18,19*).

Dissolved molecular oxygen is itself paramagnetic and shortens NMR spin lattice relaxation time. This has been exploited to explore changes in tissue oxygenation accompanying hyperoxic gas breathing, where T1-weighted signals increase with improved oxygenation (*20*), but since many factors influence T1 it is unlikely to provide a quantitative measure of PO_2.

There are biologic sequelae of hypoxia that are amenable to imaging. For example, prolonged hypoxia can lead to increased lactate in tissues and ^1H MRI can be used to image lactate. The redox state of nonprotein thiols, such as glutathione, is altered in hypoxic cells, and this can cause some radiopharmaceuticals to accumulate in hypoxia. A similar phenomenon can be measured when hypoxia results in altered adenine nucleotide redox state, NADH or NADPH. All of these tests are measuring a downstream consequence of hypoxia, and they often do not instantly return to normal after an adequate O_2 supply has been established.

HYPOXIA IN TUMORS

When otherwise healthy cells are acutely deprived of O_2, they invariably die. Tumor cells are gradually exposed to chronic hypoxia as they outgrow their vascular supply, and this can lead to an adaptation that has a negative effect on their response to treatment. If the tumor is not well perfused, chemotherapeutic drugs do not have good access to each tumor cell. Furthermore, tumor cells rapidly adapt to hypoxia by slowing their growth rate, and conventional chemotherapy generally is toxic to cells at a level that is proportional to proliferation. Most chemotherapeutic drugs are essentially antiproliferation agents rather than specific anticancer agents so that when cells enter a resting phase in their cycle, they are not sensitive to these cytotoxic agents.

Ionizing radiation is a strategy for killing proliferating cells that does not rely on vascular delivery because the radiation field is homogeneous. But the cytotoxicity of ionizing radiation depends on the level of intracellular O_2. Gray observed over 50 y ago that about a 3 times higher dose of photon irradiation is required to kill O_2-deprived cells than for well-oxygenated cells (*21*). Ionizing radiation damages DNA in several ways, most commonly by double-strand breaks from secondary radical products in the vicinity of the DNA. When the primary radical reacts with O_2, the damage is rendered permanent, whereas reaction with small thiols can repair the radical damage. This oxygen enhancement ratio (OER) transitions from 1 to 3 in the range of 2,000–5,000 ppm of O_2, below 5 mm Hg PO_2. Clinical trials of oxygen-mimetic radiosensitizers plus radiotherapy did not result in a significant improvement in outcome, perhaps because systemic drug toxicity limited the dose (*22*), although a recent meta-analysis of 50 trials involving over 7,000 patients showed a significant, albeit small, improvement in local control for head and neck cancer (*23*). A follow-up meta analysis of over 10,000 patients in 83 randomized trials based on nitroimidazoles or other oxygen-modifying procedures such as breathing hyperoxic gas showed only minor benefit and may be attributed to the inability to stratify patients based on hypoxia and select patients who might benefit from adjuvant interventions (*24*).

Radiation oncologists have devised numerous strategies to overcome the cure-limiting consequences of hypoxia, including hyperbaric oxygen, transfusion to increase Hb levels, blood substitutes that are better carriers of O_2, and others, but with little success (*23,24*). In fact the oxygen mimetics described in the next section as the basis for radiopharmaceutical imaging were one of the more effective strategies for combating tumor hypoxia (*25*). During the 1970s, the biochemistry of nitroimidazoles, small molecules with the potential to overcome the assumed mechanism of radiation resistance, was studied. When chemists started developing hypoxia imaging strategies, it was with the goal of identifying 3 factors in cancer biology that were thought to limit response to treatment: decreased blood flow and hence delivery of drugs, decreased proliferation and hence fewer cycling cells, and absence of the OER in these tumors. One of the first clinically significant contributions to radiation therapy from hypoxia imaging was the report of Rasey and Koh that oxygenation in some but not

all lung tumors was returned to normal after the first few radiation treatments (*26*).

At the same time that these imaging studies were starting to be used in clinical research, several investigators were using O_2 electrodes to measure PO_2 in accessible tumors, most commonly cervix (*27*), head and neck (*28*), and breast (*29*). These electrode studies became more convenient with FDA approval of the Eppendorf PO_2 Histograph (*7,30*), which could be used under CT guidance to collect a histogram of 50–80 PO_2 measurements along 5 or 6 tracks to obtain an overall impression of the oxygen status of a tumor. In all of the tumor types that were studied, these results showed poorer response when an appreciable fraction of the PO_2 readings were below 7–10 mm Hg. These patients had poorer local control and more metastases. By promoting metastatic spread, hypoxia can even limit cure by surgery in uterine cervical carcinoma (*27,31,32*) and soft-tissue sarcomas (*33*).

During the 1990s, the working model of the biologic significance of hypoxia in tumors became a lot more complicated. Semenza (*34,35*) worked out the detailed biochemistry involved in the molecular sensor of oxygen deprivation. His laboratory implicated hypoxia inducible factor 1 (HIF-1), as the transcription factor that leads hypoxic cells to up-regulate more than 100 proteins that promote survival and increased aggressiveness of hypoxic tumor cells. The mechanism is elegant in its simplicity. Briefly, mammalian cells along the whole evolutionary ladder constitutively express a protein that, when adequate O_2 is present, becomes hydroxylated at several proline residues and this leads to ubiquitination and proteasomal degradation (Fig. 1). However, when O_2 is absent this molecule survives as HIF-1α and translocates to the nucleus, where it forms a heterodimer with HIF-1β. The heterodimer, HIF-1, is the transcription factor that is recognized by at least 100 hypoxia response element sites on chromosomes. These sites are all characterized by the minimal motif of 5′-TACGTG-3′ of target genes, and they activate transcription of at least 100 proteins to support survival of the cancer cell (*36,37*). HIF-1 binding can also be mimicked by several oncogenic signaling pathways that bind to the same sequence, such as myc, even under normoxic conditions (*36,37*). Both insulin and insulinlike growth factor 1 induce HIF-1 activity, independent of hypoxia (*38*).

Table 1 is an abbreviated list of the HIF-1 transcription products adapted from Semenza (*35*). It includes proteins that are essential for glycolysis, a source of energy that does not require O_2 and can take place under aerobic or anaerobic conditions. Other proteins promote growth and neovascularization or induce mutations in p53 that thwart apoptosis. Still others promote metastatic spread by up-regulating proteolytic enzymes that degrade extracellular matrix (*37*) and permit cells to break away from the primary tumor as well as molecules that down-regulate the immune surveillance system (*39*). In summary, the consequences of HIF-1 are uniformly directed toward survival of the tumor and lead to a poor response to cancer treatment for reasons that go far beyond the simplistic model of hypoxia being associated with removing cells from the most sensitive part of the cell cycle, compromising access of drugs to the cancer cells, or minimizing the OER. The importance of imaging hypoxia as a resistance factor leading to poor treatment outcome has much broader implications than were appreciated when hypoxia imaging was first developed in the 1980s (*40–46*).

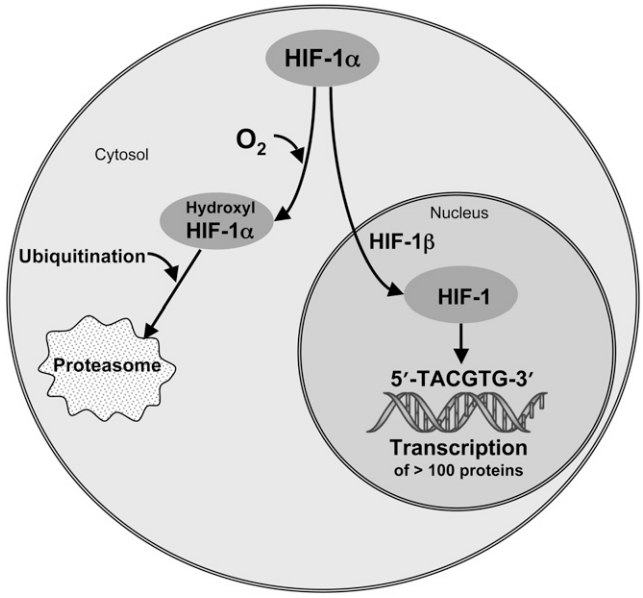

FIGURE 1. Schematic of HIF-1α pathways. HIF-1α either senses O_2 and is degraded (left pathway) or survives in absence of O_2, heterodimerizes, and binds to hypoxia response element domains (right pathway) to transcribe numerous proteins.

RADIOPHARMACEUTICAL APPROACH TO MEASURING HYPOXIA

The best way to measure hypoxia would be with a probe that competes directly with intracellular O_2, one in which the indicator was not trapped when O_2 supply was keeping up with demand but was retained when O_2 supply was inadequate to accommodate all of the electrons being produced in the electron-transport chain (Fig. 2A). Furthermore, because of the coupling between blood flow and hypoxia, the probe should be delivered to all cells equally and independent of vascular flow. There is a well-studied class of molecules that meet these criteria, the oxygen mimetics that were once evaluated as an adjunct to increase the cytotoxicity of radiation therapy. Chapman suggested the potential of imaging using radiolabeled nitroimidazoles (*40*) and he and others (*42,47–49*) showed with microautoradiographs that ^{14}C-labeled derivatives of N-alkyl-2-nitroimidazoles were trapped in cells that were hypoxic but still had electron-transport activity; that is, they were still alive. The necrotic center of tumors did not accumulate the ^{14}C, and regions of tumor that were within 100–200 μm of

TABLE 1
Genes That Are Transcriptionally Activated by HIF-1

Category	Gene(s)
Glucose metabolism	GLUT1, GLUT3
	HK1, HK2
	GPI
	PFK1, PFK2
	Aldose-A
	TPI
	GAPDH
	PGK1
	PGM
	Enolase-1
	PK-M
	LDHA
	CA9
Metastasis	CATHD
	Collagen V
	MMP2
	UPAR
	PAI1
	LRP1
	AMF/GPI
	MIC2
Cell proliferation	Cyclin G2
	IGF2
	IGF-BP
	TGF-α
	TGF-β
Cell survival/angiogenesis	ADM
	EPO
	NOS2
	VEGF
	LEP
	LRP1
Iron metabolism	Transferrin
	Tf receptor
	Ceruloplasmin
Drug resistance	MDR1

a vascular supply and were therefore well oxygenated also failed to accumulate tracer.

The mechanism by which 2-nitroimidazoles are reduced and retained in hypoxic tissues is now reasonably well understood (Fig. 2B). Several different derivatives of this structure have octanol/water partition coefficients that are close enough to 1 so that they are freely diffusible and homogeneously distributed in the body within an hour after injection at levels that reflect the tissue partition coefficient and maintain a volume of distribution essentially equal to that of total body water (*50*). This characteristic can be visually appreciated by viewing Figure 3 in the article by Lee and Scott (*46*). They are less than 5% protein bound, allowing efficient transport from blood into tissues. Therefore, their biodistribution is not complicated by reduced blood flow (*42,51,52*). The nitro functionality has an affinity for electrons, although less so than O_2. This means that a terminal e^- from the respiratory cycle can bind to the $–NO_2$ group to form the radical anion, $–NO_2^-$. A small but steady-state level of these radical ions exists wherever carbon substrates, for example, glucose or fatty acids, are being metabolized by oxidative phosphorylation to produce electrons. If O_2 is present in the cell in a concentration sufficient to compete for these extra electrons, the O_2 can accept the electron from the nitro radical, forming conventional terminal electron products and returning the nitroimidazole radiopharmaceutical to its parent state. If, on the other hand, another electron reacts with the nitro radical anion first, making the 2-electron reduction product, O_2 can no longer reverse the process. Then the labeled nitroimidazole goes on to form an alkylating agent that reacts indiscriminately with intracellular macromolecules; it is irreversibly trapped (*53*). The reduction of the nitro group on the imidazole ring is accomplished by tissue nitroreductases that are plentiful and do not represent a rate-limiting factor (*54*). Furthermore, the PO_2 where nitroimidazoles are retained in cultured cells is in the same range as that where the OER is observed (Fig. 3).

This is the molecular basis for an imaging agent that is trapped at a level proportional to the intracellular demand for O_2 and is not limited by blood flow, meeting the design requirements for a hypoxia imaging agent. 2-Nitroimidazoles are most commonly labeled with PET radionuclides such as ^{18}F or ^{124}I (*42,55*) but can also be labeled with single-photon emitters, such as ^{123}I (*45,56*) or even ^{99m}Tc (*45,57,58*), or with multiple ^{19}F atoms for detection by MRI (*59,60*). Because of their long history, this review provides substantial detail on labeled nitroimidazoles for PET, especially fluoromisonidazole, the most widely studied hypoxia imaging agent (*46*).

PHARMACOLOGY AND BIOCHEMISTRY OF NITROIMIDAZOLES

Nitroimidazoles have been studied extensively as oxygen mimetics designed to increase the cytotoxicity of ionizing radiation in tissues with low O_2 concentration. Much of this research took place in the 1970s and 1980s and has been critically reviewed by several authors (*61,62*). Metabolism of misonidazole (MISO) is similar to that of fluoromisonidazole (FMISO). Several intracellular nitroreductase enzymes (including xanthine oxidase, lipoxygenases and NADPH oxidases) lead to the single-electron product that is the basis for the imaging strategy. There are other metabolic reactions that occur in vivo and lead to products that contribute to background but do not indicate hypoxia signal. In vivo under normal oxygen tension, MISO is metabolized primarily in the liver to its desmethylated derivative, but this reaction cannot occur with FMISO because it lacks the methoxy substituent. From 7% (humans) to 14% (mice) is conjugated to the glucuronide and less than 5% is reduced to aminoimidazole. Substantial amounts of MISO are recoverable in feces, and fecal anaerobic bacteria can reduce misonidazole in the absence of oxygen (*42*). Both FMISO and MISO have similar body clearance, and their

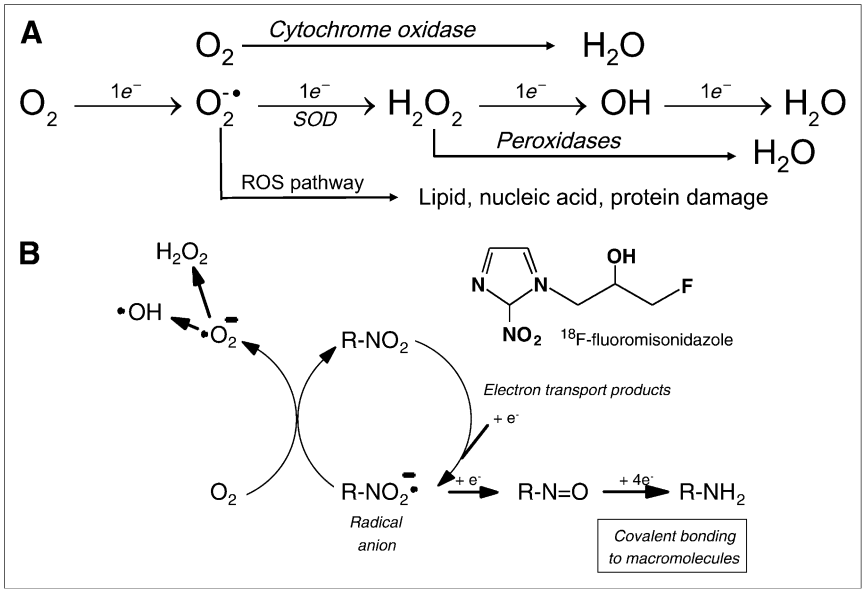

FIGURE 2. (A) Molecular oxygen is terminal electron acceptor in mitochondrial respiratory chain. Electrons mostly react with O_2 to form H_2O in a process catalyzed by cytochrome c oxidase, complex IV. Some e^- escape and combine with O_2 to form superoxide radical anion, which reacts with superoxide dismutase (SOD), which is abundant in anaerobic organisms; alternatively, reactive oxygen species (ROS) oxidize critical biomolecules, leading to cellular dysfunction and death. H_2O_2 is substrate for catalase and peroxidase enzymes and eventually produces more H_2O. (B) Mechanism of reduction and intracellular retention of nitroimidazoles involves buildup of steady-state level of 1 e^- radical anion, which reacts preferentially with O_2 if it is present to return tracer to its original form. If O_2 is not present, it accepts another e^- to produce intermediate that is sequentially reduced to highly efficient alkylating agent, RNH_2, resulting in cellular retention of labeled tracer.

metabolites are primarily excreted in the urine (*42,63,64*). No measurable amounts of defluorinated metabolites from FMISO were found in plasma or urine at 4 h after injection (*51*).

Our knowledge of the toxic effects of 2-nitroimidazoles in humans is based on misonidazole, a close analog of FMISO. The plasma half-life of FMISO in humans is similar to MISO as they have similar sizes and partition coefficients and both are cleared primarily through the kidneys. The therapeutic potential of nitroimidazole radiosensitizers has been studied in over 7,000 patients in 50 randomized trials as reviewed by Overgaard (*23*). Oral MISO was the agent in 40 trials involving 5,377 patients. The maximum doses used were 4 g/m^2 in a single dose and 12 g/m^2 as a total dose. Clinical studies using multiple dosing of MISO have reported that peripheral neuropathy with a latency period of several weeks was the manifestation of toxicity that became dose-limiting with daily oral doses of over 3 g/m^2 (*65*). Limiting the total dose and giving no more than 2 doses in 1 wk minimized neuropathy. Nausea, vomiting, skin rashes, ototoxicity, flushing, and malaise have also been reported (*66*). Patients receiving up to 140 mg/kg tolerated the drug well. Neuropathies were generally, but not always, reversible when the drug was discontinued. There have been 2 fatalities attributed to misonidazole (*62*). Both patients had advanced malignant disease and died in convulsions; one patient received 51 g orally in 17 d, 6 fractions, and the other had 16 g in 3 d, 2 fractions.

Projections based on the interspecies pharmacokinetic models of Paget (*67*) rely on similarities among related chemical entities. The octanol/water partition coefficients for MISO and FMISO are both 0.4; the LD50s in adult male BALB/C mice for MISO and FMISO are 1.8 mg/g and 0.9 mg/g, respectively (*50*). Using the relative toxicity factors from Paget of 1.0 for mice and 9.8 for humans, the projected LD50 values for a 70-kg person are about 12.5 g for MISO and 6.5 g for FMISO. This MISO value is consistent with the findings from the early clinical trials.

The dose to humans in initial FMISO nuclear imaging protocols was as high as 1 mg/kg, approximately 0.1% of the calculated LD50. Total patient imaging dose for the current radiopharmaceutical formulation is less than 15 μg. That the drug has no adverse effects at these doses can be confidently stated as a result of the 5,377 patients treated with MISO (*23*) and the growing literature reports of imaging studies with several nitroimidazole derivatives for nuclear, magnetic resonance and immunohistochemical detection.

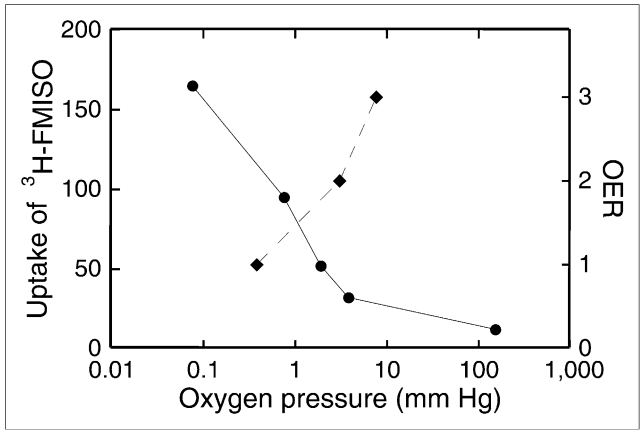

FIGURE 3. Uptake (arbitrary units) of ^{3}H-FMISO increases by greater than 20-fold at low PO_2 (left axis and solid line). This process occurs at approximately same O_2 pressure at which oxygen enhancement effect (right axis and dashed line) decreases from its normoxic value of about 3 to its hypoxic value of about 1. OER is ratio and thus has no units. These experiments involved cells in cultures.

Fluoromisonidazole: Preclinical Studies

Uptake of FMISO by multicellular spheroids, aggregates of cells that grow in culture and mimic small tumors, provided a visual and a quantitative measure of hypoxia. Autoradiographs of 0.8-mm V79 spheroids after 4 h of incubation with ^{3}H-FMISO revealed heavily labeled cells in an intermediate zone between the well-oxygenated periphery and the necrotic center (Fig. 4) (*68*). The relationship between O_2 concentration and ^{3}H-FMISO binding was also studied in monolayer preparations of isolated adult rat myocytes (*69*). Under anoxic conditions, ^{3}H-FMISO binding after 3 h was approximately 25-fold greater than normoxic controls. This level of binding was reduced to 40% at a PO_2 of ~4 mm Hg. ^{3}H-FMISO uptake was not influenced by glucose or thiol concentrations or by cellular pH, potential confounding variables in the tumor microenvironment (*42,54*).

Regional variation in hypoxia within a single tumor has been observed and might result from differences in delivery of the radiopharmaceutical as well as PO_2. To investigate the ability to separate these 2 effects, relative blood flow was measured in tumors and in several normal tissues of mice by sacrificing the mice a few seconds after injection of the freely diffusible blood flow tracer, ^{14}C-iodoantipyrine, that has the same partition coefficient as FMISO. Relative flow was compared with distribution of FMISO injected 4 h earlier. Each tumor was dissected into several pieces representing central and peripheral regions, and multiple samples were taken from several normal organs (*42*). The relative blood flow measurements confirmed that the tumors had generally low flow and the highest flows were in lung and kidney. In individual tumors there was no correlation between regional flow and regional FMISO retention. The same lack of correlation was also found in normal tissues. The conclusion that FMISO uptake is independent of blood flow, even at very low flow, has been confirmed in larger animals (*52,70*).

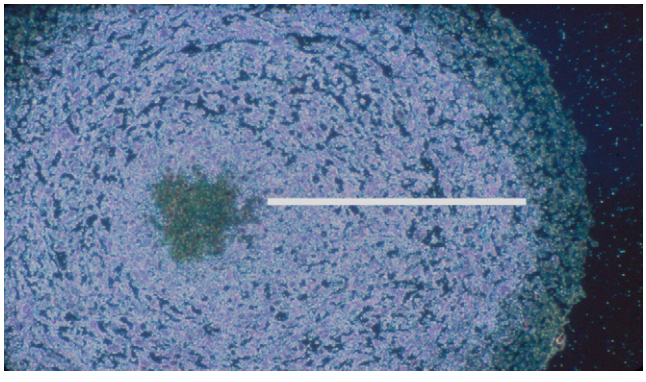

FIGURE 4. Microautoradiograph of EMT6 spheroid exposed to ^{3}H-FMISO in normoxic cell culture medium. Tritium appears as white speckles. There is no radioactivity in necrotic center, where cells have died, and there is no electron transport. Also, there is no more activity in peripheral ~150-μm layer than there is in medium. Activity is uniformly intense in hypoxic donut (bisected by white line), where cell distance from oxygenated medium exceeds O_2 diffusion limit.

Fluoromisonidazole and Related Nitroimidazoles: Clinical Studies

^{18}F-fluoromisonidazole [1-(2-nitroimidazolyl)-2-hydroxy-3-fluoropropane; ^{18}F-FMISO], is the most widely used PET agent for mapping regional hypoxia. It was originally prepared by reacting 2-nitroimidazole with the volatile precursor, ^{18}F-fluoroepihydrin (*71,72*), but this procedure was soon replaced by a more convenient nucleophilic displacement method (Fig. 5) (*73*) that is procedurally similar to preparing ^{18}F-FDG. This method is now the basis for an IND sponsored by NCI-CIP for clinical trials using ^{18}F-FMISO (*74*). Typical radiosynthesis yields are 3 GBq starting from 11.1 GBq of ^{18}F-fluoride in target water. The synthesis, including semipreparative high-performance liquid chromatography (10 μm of C18 eluted with 5% ethanol in water), takes about 35 min, and the product is collected in 5% ethanol (US Pharmacopeia) in sterile water for injection (US Pharmacopeia). In our hands, the specific activity is typically 250 GBq/μmol, and a patient injection of 260 MBq always involves the administration of less than 15 μg of ^{18}F-FMISO, typically 0.2 μg. Although the initial synthesis provided an optically active diastereomer (*72*), the product from the racemic precursor (*75*) has the same biodistribution characteristics as the pure enantiomer (*76*).

The ^{18}F-FMISO imaging protocol is similar to a bone scan protocol, with which cancer patients are generally familiar. Patients do not need to fast before the study. The desired dose of ^{18}F-FMISO is injected, and the patient is asked to return to the nuclear medicine clinic in about 1.5 h An attenuation-corrected image is collected beginning about 90–120 min after the radiopharmaceutical was injected and for sufficient time to collect enough emission events to provide a good-quality image, typically 20 min. This timing is selected to ensure that the tracer has equilibrated proportionally to the partition coefficient in blood and tissue. A venous blood sample is drawn during the imaging session, and the static image data in units of Bq/cm^3 are normalized to the ^{18}F concentration in the blood, Bq/mL, to provide a normalized map of tissue-to-blood ratio, T/B, for each pixel in the image. Because ^{18}F-FMISO partitions nearly equally between octanol and water, normoxic tissues have T/B pixel values of almost 1.0. When the O_2 supply is

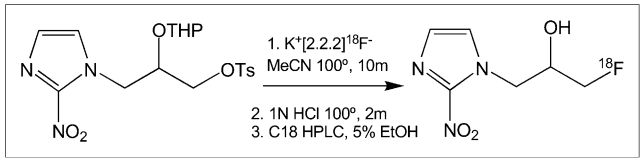

FIGURE 5. Schematic for radiochemical synthesis of ^{18}F-FMISO. EtOH = ethanol; HPLC = high-performance liquid chromatography; MeCN = acetonitrile; OTHP = *O*-tetrahydropyranyl; OTs = *O*-toluene sulfonyl.

adequate, most tissues have the same level of ^{18}F as is in the blood. Because of the partitioning mechanism, whole-body clearance of ^{18}F-FMISO is slow. Thus, the contrast is not high in raw ^{18}F-FMISO images, and ^{18}F-FMISO PET has been criticized for this reason. However, the fact that pixels with a T/B of less than 1 are reliably normoxic allows for unambiguous visualization of regions that are truly hypoxic.

The hypoxic part of a tumor can be characterized by the maximum T/B value or by the total number of pixels with T/B greater than some threshold. These pixels can be summed and multiplied by the known mL/pixel to calculate a hypoxic volume, HV. Although these 2 parameters should be expected to covary, the T/B_{max} indicates the greatest level of hypoxia in the tumor whereas the HV indicates the total volume of tumor that is hypoxic. The relative predictive value of these 2 parameters is under investigation.

The uptake of ^{18}F-FMISO in normal human tissues has been measured and used to estimate the radiation-absorbed dose (*77*). All tissues demonstrated a rapid uptake phase followed by exponential clearance, and all tissues received a similar radiation dose, reflecting the similarity of biodistribution to that of water (*50*). Estimated total-body absorbed dose for a 70-kg man injected with 3.7 MBq/kg is 0.013 mSv/MBq; for a woman it is 0.014 mSv/MBq. The radiation exposure from ^{18}F-FMISO is equal to or lower than those from other widely used radiopharmaceuticals.

Positron emission scanning with ^{18}F-FMISO has been studied widely over the past 15 y. The general conclusion from these studies is that ^{18}F-FMISO PET identifies hypoxic tissue that is heterogeneously distributed within human tumors (*42,78*) and promises to help facilitate image-directed radiotherapy (*79,80*) and clinical trials of new hypoxia-selective cytotoxins (*81*) as ways to circumvent the cure-limiting effects of tumor hypoxia. In addition, ^{18}F-FMISO has identified a discrepancy between perfusion, blood–brain barrier disruption, and hypoxia in brain tumors (*82*) and a lack of correlation between ^{18}F-FDG metabolism and hypoxia in several types of malignancies (*83–87*). Hypoxic tissue does not correlate either with tumor volume or vascular endothelial growth factor (VEGF) expression (*83,88*). ^{18}F-FMISO imaging was used to identify post-radiotherapy tumor recurrence by differential uptake of tracer. The standardized uptake value (SUV) ratio between recurrent tumor and muscle was greater than 1.6 and between tumor and normal mediastinum was greater than 2.0 (*89*). Only one study has concluded that ^{18}F-FMISO was not "feasible for the detection of tumor hypoxia in human soft-tissue tumors" (*90*), although hypoxia imaging was developed to characterize tumors, not for detection.

Nuclear medicine methods for imaging hypoxia in patients with cancer have been reviewed in several publications (*42–46,78*). Although its clinical role is still being assessed, ^{18}F-FMISO has been established as a robust radiopharmaceutical for obtaining images to quantify hypoxia using PET, and it remains the single most commonly used agent for imaging hypoxia. Although its biodistribution properties do not result in high-contrast images, they result in an image at about 2 h after injection that unambiguously reflects regional PO_2 in the range where it is clinically significant. In human metastatic neck lymph nodes, comparison of the ^{18}F-FMISO tumor-to-muscle uptake ratio at 2 h and Eppendorf PO_2 histography found an average to high correlation; not surprisingly, no correlation was found with ^{18}F-FDG (*85*). Studies have shown that a level of hypoxia higher than the median value is predictive of poor locoregional control and a higher rate of metastatic spread. In head-to-head comparisons of ^{18}F-FDG and ^{18}F-FMISO imaging, ^{18}F-FMISO was a stronger predictor of outcome than ^{18}F-FDG and it had independent value (*91*). A significant correlation was found between hypoxic tissue identified by ^{18}F-FMISO and both pimonidazole and carbonic anhydrase IX, CA9, detected by immunohistochemical staining techniques (*92*), although other investigations have questioned the validity of CA9 as a reference standard for hypoxia (*93*). A recent critical review of ^{18}F-FMISO PET provides a useful summary of results from several clinical studies involving over 300 patients (*46*). It concluded that ^{18}F-FMISO has been validated in multiple studies and is "gaining increasing importance for its potential to predict response to treatment and provide prognosis in a wide range of pathologic processes."

Several alternative nitroimidazole derivatives have been described with the goal of a possibly more optimal partition coefficient and therefore faster clearance properties, less nonspecific retention, or fewer metabolites. Motivation for developing new nitroimidazole radiopharmaceuticals came from a report of metabolites in the urine and plasma of mice injected with ^{18}F-FMISO (*94*) and a desire to accelerate whole-body clearance of the radiopharmaceutical. Although the mouse study showed 5% metabolites for ^{18}F-FMISO after 2 h, no time course for metabolism has been reported and the total amount in plasma at 2 h, inferred from the blood clearance data in the same paper, suggests that under the worst case less than 5% of the total injected dose was plasma metabolite. Metabolite levels have not, to the best of our knowledge, been reported in human studies sufficient to require a correction of the input function for metabolism.

Several alternative reagents are summarized in Figure 6 and Table 2 and have been evaluated as imaging agents in single-center pilot studies (*45*). A study from Finland reported using ^{18}F-fluoroerythronitroimidazole (^{18}F-FETNIM) to evaluate 10 patients with head and neck squamous cell cancer at doses of about 370 MBq without adverse effects (*95*). FETNIM was found to be equivalent to ^{18}F-FMISO both in correlation with oxygenation status and in tumor-to-muscle uptake ratios in mice with implanted C3H mammary carcinomas (*96*). Other agents, fluoropropylnitroimidazole and fluorooctylnitroimidazole, have not proved as useful in visualizing hypoxic tissue (*97*), probably because of their greater lipophilicity than ^{18}F-FMISO.

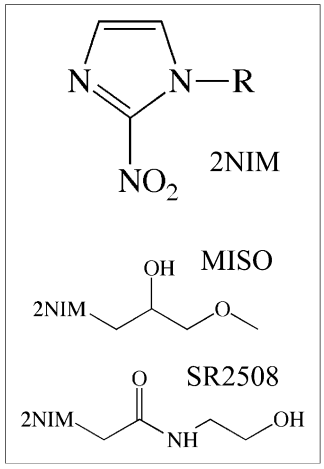

FIGURE 6. Structures of 2-nitroimidazole (2NIM), which are either secondary alcohols or amides. See Table 2 for more information.

A derivative that is more hydrophilic than ^{18}F-FMISO, ^{18}F-fluoroazomycin-arabinofuranoside (^{18}F-FAZA), had been recommended for further study (*98,99*) and shows considerable clinical promise. ^{18}F-FAZA and ^{18}F-FMISO were compared in 2 murine tumor models, and the tumor-to-muscle and tumor-to-blood ratios were higher for ^{18}F-FAZA at all times, reflecting its somewhat faster clearance (*100*). A related derivative has been proposed, ^{124}I-iodoazomycin galactoside, and was an effective imaging agent in some animal studies (*101*). The long nuclear half-life of ^{124}I allows imaging at 24–48 h after administration, a time when much of the body background has cleared. Although this might be a way to minimize the effect of blood flow on hypoxia images, the requirement that patients return a day later would be a practical deterrent.

^{18}F-fluoroetanidazole (^{18}F-FETA) is yet another 2-nitroimidazole that shows promise as a hypoxia imaging agent. This molecule was first developed to circumvent some of the metabolic side reactions of ^{18}F-FMISO in vivo where most of the ^{18}F in the urine was not ^{18}F-FMISO (*94*). A careful biologic evaluation of ^{18}F-FETA found that this second-generation agent had potential advantageous physicochemical properties. Most notably it was stable to nonhypoxic degradation in vivo (*102*). Tumor retention of ^{18}F-FETA reflected tissue PO_2 in the same range as with^{18}F-FMISO, 1–10 mm Hg. Its overall clinical value remains undefined at this time.

TABLE 2
Alkyl Substituents Affecting Partition Coefficients of 2-Nitroimidazole Imaging Agents

Name	-R structure	Partition coefficient*
SR2508	$-CH_2CONHCH_2CH_2OH$	0.046
FETA	$-CH_2CONHCH_2CH_2F$	0.16
FETNIM	$-CH_2CHOHCHOHCH_2F$	0.17
MISO	$-CH_2CHOHCH_2OCH_3$	0.43
FMISO	$-CH_2CHOHCH_2F$	0.44 (0.41)
EF1	$-CH_2CONHCH_2CH_2CH_2F$	0.20
EF3	$-CH_2CONHCH_2CH_2CF_3$	1.25
TF-MISO	$-CH_2CHOHCH_2OCH_2CF_3$	2.6
EF5	$-CH_2CONHCH_2CF_2CF_3$	5.7

*Octanol/water value.

The more highly fluorinated 2-nitroimidazoles that were first developed for ^{19}F NMR studies, described later, have been radiolabeled with ^{18}F and evaluated as PET agents. These molecules are fluoroalkyl acetamide derivatives and have been abbreviated EF1 (*103*), EF3 (*104*), and EF5 (*105*). Within this family, EF5 has been thoroughly validated using drug adducts that can be detected by immunohistochemistry. A multicenter clinical trial to test EF5 as a hypoxia imaging agent is about to begin. Although there have not been any direct comparisons with ^{18}F-FMISO PET, comparisons with pimonidazole and pharmacokinetic studies establish it as similar to ^{18}F-FMISO. One possible disadvantage of ^{18}F-EF5 is that the labeling chemistry is more complex than the simple nucleophilic displacement reactions used for the mono-fluorinated 2-nitroimidazoles (*106*).

Several single-photon–emitting radiolabels have been evaluated for labeling nitroimidazoles, including ^{123}I and ^{99m}Tc. This research has been covered in recent reviews (*43,45,57*) and will not be described here as single-photon agents for imaging hypoxia have not found a clinical role.

In summary, it remains unclear whether any of the alternative 2-nitroimidazoles provides sufficient advantages over ^{18}F-FMISO for a dominant role in clinical trials using nuclear imaging, given the substantial human experience with ^{18}F-FMISO. The reality, perhaps unfortunate, is that once an imaging agent develops a clinical history with several hundred patients, a new agent has to be substantially superior to gain acceptance. Alternatively, it may be that several of the 2-nitroimidazoles with partition coefficients within a log unit of water will provide equivalent imaging results and could be combined in clinical trials. Perhaps we now have too many potential hypoxia tracers. We would argue that it is time to show whether imaging hypoxia is useful to the oncology community rather than developing more radiopharmaceuticals with marginally improved pharmacokinetic properties.

Cu-ATSM IMAGING OF HYPOXIA

An alternative PET agent for hypoxia is based on a metal complex of radioactive copper with ATSM, diacetyl-bis(N^4-methylthiosemicarbazone) (*44,107*). Dithiosemicarbazones have antitumor properties that are enhanced when they are complexed with Cu(II). Because there are several advantageous imaging radionuclides of copper, this has led several laboratories to develop substituted ligands of dithiosemicarbazones as potential imaging agents (*108*). The first of these had 3 methyl substituents, PTSM, and was promoted as a blood flow agent (*109*). When another methyl was added to the diimine backbone, the Cu(II) complex was found to accumulate in hypoxic myocardium (*107*). The

additional methyl had a minor effect on partition coefficient but a more substantial effect on reduction potential, $E_{1/2}$, for Cu(II) → Cu(I). Testing in several tumor cell lines showed that uptake increased nearly 3x when cultured cells went from a PO_2 of about 5 mm Hg down to less than 1 mm Hg, the radiobiologically significant range. Unfortunately, this hypoxic effect was not shown in all cell lines, and some cell lines showed no hypoxic selectivity at all (*110,111*). Furthermore, in a direct comparison involving Cu-ATSM, ^{18}F-FMISO and pimonidazole in the SCCVII tumor model that has been widely used for studies of oxygenation effects, uptake of both ^{18}F-FMISO and pimonidazole decreased as oxygenation increased, as would be expected for a hypoxia imaging agent, but uptake of Cu-ATSM increased under the same conditions (*112*).

These results led independent laboratories to study the mechanism of retention of Cu(II)-ATSM in some hypoxic cells. The approach involved a structure activity study of 13 ^{64}Cu-bis-thiosemicarbazones that differed only in number and location of alkyl or aryl substituents. The log P for this series ranged from 0.45 to 2.69 and $E_{1/2}$ for Cu(II/I) ranged from −0.31 to −0.59 V with respect to a standard Ag electrode. The copper reduction reaction was monitored with a combination of cyclic voltammetry over a range of pH, optical spectrometry, and density function calculations. Alternative mechanistic arguments based on this work were critically reviewed by Vavera and Lewis (*108*). The simple mechanism is that reduction of Cu(II)-ATSM to Cu(I)-ATSM takes place continuously in both normoxic and hypoxic cells, but in the presence of O_2 the copper is rapidly reoxidized to Cu(II)-ATSM which can freely diffuse in and out of cells. Cu(I)-ATSM is charged and trapped and may dissociate and transfer the radiocopper to other intracellular macromolecules. This is an attractive mechanism but fails to account for the variability with tumor type. Furthermore, it would not reconcile the paradoxical increase in Cu-ATSM uptake as PO_2 increased after an episode of hypoxia. A recent review recommends additional studies be performed to deconvolute the copper reduction reaction from the basic coordination chemistry (*108*). Alternatively, it may be that changes in the thiol redox chemistry that occur as sequelae of hypoxia and HIF-1 activation are complicating the retention mechanism. Additional research elucidating the biochemical reasons why Cu-ATSM accumulates in tumors is urgently needed.

Preclinical studies with ^{62}Cu-ATSM have shown that it is reduced and retained in hypoxic tissues, whereas it rapidly washes out of normoxic tissues (*107*). Cu-ATSM uptake is more rapid than ^{18}F-FMISO uptake, and the reported hypoxic-to-normoxic ratio is greater (*113–115*). This is thought to reflect greater membrane permeability or more rapid blood clearance, although permeability is probably not the reason because early ^{18}F-FMISO images accurately measure blood flow (*70*) and the image contrast of several 2-nitroimidazoles ranging over a wide value of partition coefficients is equivalent. Furthermore, the partition coefficients of Cu-ATSM and Cu-PTSM are essentially identical. The greater concern is that, because of its lipophilicity, the early uptake and washout of Cu-ATSM is probably influenced by regional blood flow, which is a major confounder with hypoxia.

Nevertheless, Cu-ATSM is finding a useful role in several clinical settings. In an initial study of 14 patients with biopsy-proven non–small cell lung cancer, ^{60}Cu-ATSM uptake predicted response to therapy with radiation or chemotherapy (*116*). A more recent clinical study reported imaging of 15 patients with cancer of the uterine cervix who were imaged with ^{60}Cu-ATSM (*117*). In this study, 481 MBq of ^{60}Cu-ATSM were injected intravenously, followed by a 60-min dynamic imaging study. Uptake was assessed semiquantitatively by determining the tumor-to-muscle ratio from the summed 40- to 60-min data, as well as from a parametric map of a rate parameter. The rate and ratio data lead to the same conclusions, so the simpler ratio method was preferred and a threshold ratio of 3.5 was found to be an accurate cutoff for defining clinically significant hypoxia (*118*). In the cervical cancer study, Cox proportional hazards modeling demonstrated that hypoxia as determined by the PET images was a significant independent predictor of tumor recurrence. Four-year overall survival estimates were 75% for patients when the Cu-ATSM PET study was negative and 33% when it was positive. In this pilot study, the PET results were compared with several biomarkers linked with hypoxia: VEGF, COX2, EGFR, CA9, and apoptotic index, with the result that only CA9 and apoptosis were significant at $P < 0.05$ (*117*). VEGF was the poorest correlate of hypoxia. Although these patient numbers were small, the results clearly suggest further clinical evaluation is warranted, and some positive results should be expected within the next few years.

DIRECT MRI METHODS FOR MEASURING HYPOXIA

MRI methods for interrogating tumor oxygenation are attractive since they avoid the complication of short-lived radioactivity and MRI equipment is widely available. The most facile approach avoids the need for reporter molecules by imaging differences between O_2Hb and deoxyhemoglobin (dHb), which is paramagnetic and increases the R_2* (=1/T_2*) relaxation rate of blood water. Changes in dHb are revealed by signal gain in T2*-weighted images, such as accompanying hyperoxic gas breathing, which increases vascular delivery of oxygen. BOLD MRI signal is related to vascular oxygenation and may allow direct estimates of PO_2, for example, in the superior mesenteric vein or heart of children (*119,120*). However, the correlation becomes difficult for smaller blood vessels where partial-volume effects combine vessel and tissue in individual voxels (*121*). BOLD may also be confounded by flow effects, although appropriate pulse sequences can be used to minimize these. Howe et al. coined the term "FLOOD" to describe flow- and oxygen-dependent contrast using pulse sequences to decouple flow effects from the static effects of R_2* (*122,123*). A correlation between BOLD and PO_2

response in tumors has been reported (*124*). Baudelet and Gallez have rigorously investigated correlations between PO_2 estimated using fiber optic probes and BOLD signal changes and have found general correlations, but a given BOLD response may reflect vastly different changes in PO_2 (*125*). BOLD MRI has the advantage of both high spatial and temporal resolution and it can be repeated as needed. It is particularly attractive to patients, and IRBs rapidly accept oxygen breathing during MRI.

Historically, radiation biologists favored breathing carbogen (95% O_2/5% CO_2) over oxygen (100% O_2) as an adjuvant intervention to reduce tumor hypoxia. Indeed, oxygen may alter hemodynamic parameters, potentially inducing hypotension with possible reduced delivery of oxygen to tumors with high interstitial pressure. Carbogen was used as part of the ARCON trial, which was reported to be successful (*126,127*). However, carbogen can cause respiratory distress in patients and is not always well tolerated. A lower CO_2 content (2%) still modulates PO_2 and with less patient discomfort (*128*). In our own studies, we generally found very similar results using oxygen or carbogen to modify tumor PO_2 (*129–133*). Because of the differential effects of hyperoxic and hypercarbic gases, depending on vascular maturity (*134*), it appears that these gases deserve further evaluation with respect to BOLD studies in patients. To date, BOLD investigations have been largely exploratory in terms of methods of implementation. As a caution, they can be susceptible to motion artifacts that may be subtle (*44*).

BOLD studies have been reported in diverse human tumors (*135–138*). Rijpkema et al. used BOLD to evaluate patients during the ARCON trial for head and neck cancer and found significant changes in T2*-weighted MRI contrast accompanying hyperoxic gas breathing (*128*). No accompanying changes were observed by traditional T1-weighted Gd-DTPA dynamic contrast-enhanced MRI. At the San Antonio breast cancer meeting, preliminary data were presented for a group of 10 women being treated with chemotherapy for locally advanced breast cancer. There were a significantly different BOLD response to breathing oxygen before the course of chemotherapy for tumors of women with good therapeutic outcome versus those with poor response. Indeed, 3 women with complete pathologic response showed a signal change greater than 7%, whereas those with poor outcome showed less than 3% (*139*). It is not yet clear whether the differential response reflects perfusion or oxygenation, but traditional dynamic contrast-enhanced MRI failed to provide similar discrimination.

REPORTER MOLECULES FOR MR OXIMETRY

Oxygen-sensitive MR reporter molecules have also been developed, generally based on perfluorocarbons (PFCs). In this method, there is a linear relationship between $R = 1/T_1$ of the ^{19}F signal, and PO_2 and calibration curves obtained in vitro are valid in vivo (*140*). Indeed, the extreme hydrophobicity of PFCs ensures that gases are highly soluble, providing molecular amplification of O_2 concentration while ions are repelled and do not perturb the relation (*141*). Originally, perfluorocarbon emulsion blood substitutes were exploited, and Thomas et al. pioneered their application to assess vascular and tissue oxygenation (*142,143*). Although MR effects could be observed immediately after intravenous administration of PFCs, measurements were subject to flow artifacts (*144*). More generally, materials were administered intravenously or intraperitoneally and measurements were performed after complete vascular clearance. About 90% of the emulsion was sequestered in the reticuloendothelial system because of macrophage accumulation, and this approach allowed measurements of dynamic changes in PO_2 in the liver, spleen, and even bone marrow (*145–147*). However, to achieve a sufficient signal-to-noise ratio for measurements in a reasonable time in tumors or the myocardium required administration of large quantities of PFC emulsion. This led to substantial hepatomegaly and splenomegaly and was unsatisfactory for general application (*148,149*). Moreover, PFC signal was often detected from the tumor periphery, corresponding to only the most well-perfused regions (*150*). These regions are typically the best oxygenated and thus the least important in terms of tumor response to oxygen-dependent therapy. Animal studies have been reported examining changes in PO_2 in response to interventions such as breathing hyperoxic gas (*129,131,133,151–154*).

The traditional PFCs such as perfluorotributylamine have long-term tissue retention; half-life in liver may exceed 40 d. This has the advantage of allowing investigations of chronic long-term changes in PO_2 over a period of weeks without readministering reporter molecule. Progressive hypoxia in tumors during growth over a period of 2 wk can be observed (*150,155*). Many blood substitute emulsions were based on materials with multiresonant spectra (e.g., perfluorotributylamine, perfluorotripropylamine, and perfluorooctyl bromide), which complicated the imaging experiment, usually leading to signal loss. The discovery of PFCs with a single signal improved signal-to-noise ratio. Mason et al. have favored hexafluorobenzene, C_6F_6 (*156*). Because of its high vapor pressure, C_6F_6 does not form effective emulsions but may be injected directly into tumors. Based on injections of 50 μL of pure C_6F_6, maps of PO_2 may be obtained in rat tumors (Fig. 7) using echoplanar imaging in a method termed FREDOM (fluorocarbon relaxometry using echoplanar imaging for dynamic oxygen mapping) (*15*). The precision of measurements depends on the PO_2 value, with better precision for the crucial low values and estimated precision of 1–3 mm Hg when PO_2 is less than 5 mm Hg (*15*).

In developing any new assay, validation is crucial. Studies have shown that baseline PO_2 measured using FREDOM is similar to that obtained using the Eppendorf histograph (*157*). Dynamic changes in PO_2 response to interventions are commensurate with observations using

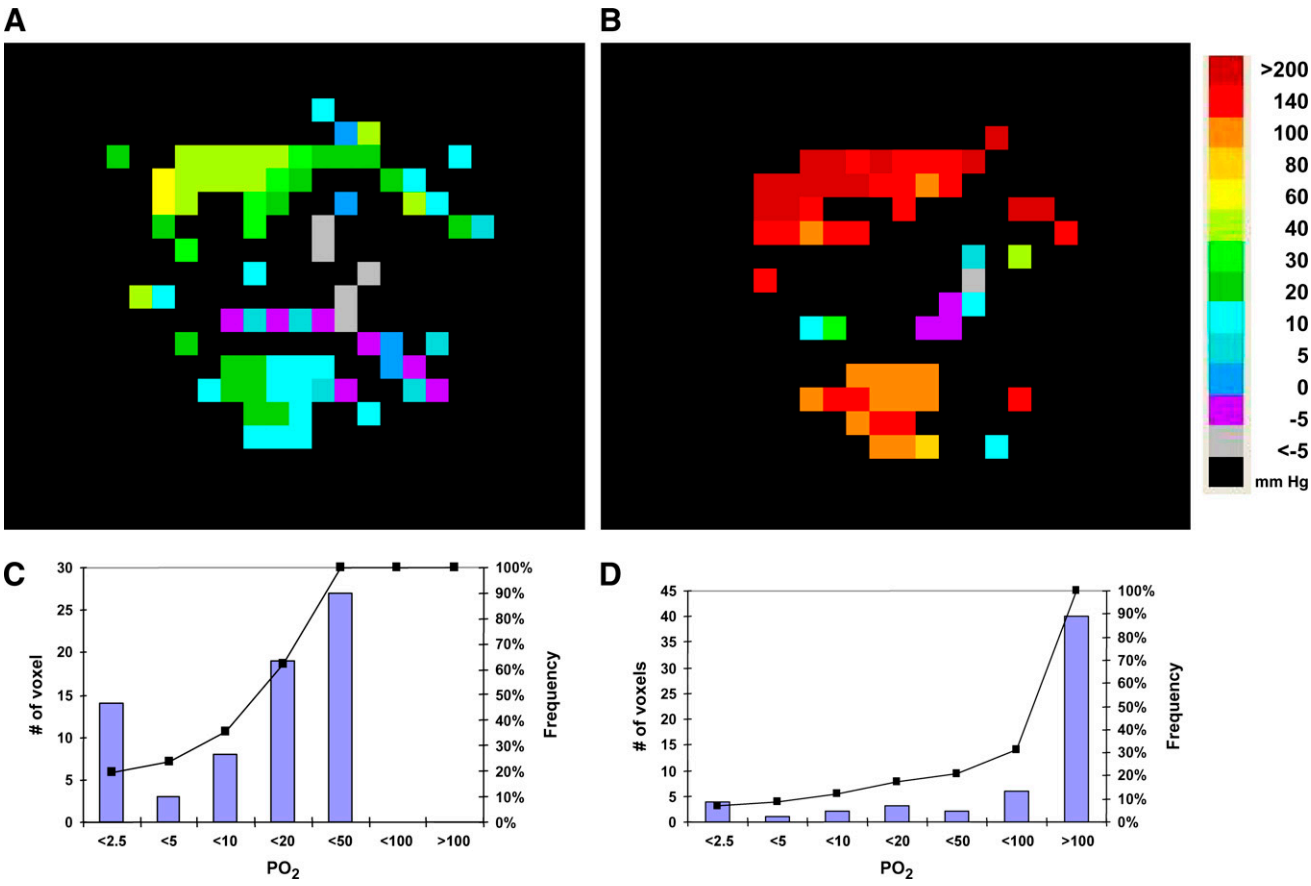

FIGURE 7. ^{19}F MRI oximetry of H460 human tumor xenograft implanted in nude rat. (A) Hexafluorobenzene (50 μL) was injected along multiple tracks directly into 0.57-cm^3 tumor growing in thigh. FREDOM was used to acquire PO_2 maps with in-plane resolution of 1.25 mm (5 mm thick) for 6.5 min each while anesthetized (1.5% isoflurane) rat breathed air and then after transition to breathing oxygen. Color maps show PO_2 ranging from hypoxia to about 60 mm Hg at baseline, but with distinct spatial heterogeneity. (B) After switch to oxygen breathing for about 15 min, PO_2 increased significantly, with many regions exceeding 60 mm Hg and hypoxia being essentially eliminated. Corresponding histograms are for air (C) and oxygen (D) breathing and show shift to right and essentially elimination of hypoxia in this responsive tumor. Cumulative frequency is overlaid on histograms.

polarographic oxygen electrodes (*132*) or the OxyLite and FOXY fiber optic probes (*13,158*). Moreover, relative hypoxia evaluated using pimonidazole and immunohistochemistry after tumor excision corresponded with baseline PO_2 observed by FREDOM before sacrifice (*159*). The FREDOM approach has been applied to diverse rodent tumors and human tumor xenografts in mice (*129,152,158–160*). FREDOM has revealed distinct heterogeneity within and between tumors, both under baseline conditions and in response to interventions. Correlations have been shown in 2 Dunning prostate rat tumor lines between tumor PO_2 at the time of irradiation and response to a single high dose of radiation. Furthermore, response to radiation can be modulated depending on the ability to alter hypoxia by breathing hyperoxic gas (Fig. 8) (*160,161*).

Extensive toxicologic literature suggests that C_6F_6 could be used in patients once GMP is applied. Indeed, the LD50 has been found to exceed 25 g/kg (*162–164*). Perhaps the major obstacle to implementing ^{19}F MRI in the clinic is the continued lack of availability of ^{19}F NMR capabilities on human MRI systems, though it is increasingly becoming available in major clinical centers.

Given the current lack of availability of MRI systems capable of imaging ^{19}F in humans, an analogous proton NMR approach (PISTOL [proton imaging of silanes for tissue oxygen levels]) has been proposed and tested in preliminary studies (*165*). Hexamethyldisiloxane (HMDSO) has properties closely matching C_6F_6 in terms of strong hydrophobicity, high oxygen solubility, low toxicity, ready availability, and inertness. Like C_6F_6, it exhibits a single NMR resonance whose spin lattice relaxation rate is sensitive to PO_2. The chemical shift is about as far from water (4.7 ppm) and fat (1.3 ppm) as possible, occurring at about 0 ppm like the traditional proton NMR chemical shift standard tetramethylsilane. Water and fat suppression readily reveal HMDSO, which can be used to interrogate tissue PO_2 after direct intratumoral injection. To date, results have been reported using NMR spectroscopy and imaging (*165*), and it remains to be evaluated with respect to therapeutic outcome. It is less volatile than C_6F_6, so HMDSO remains

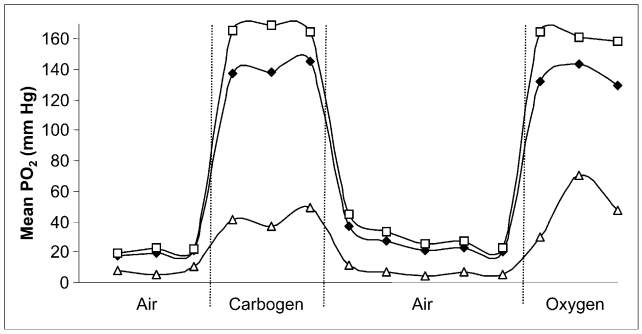

FIGURE 8. Dynamic oximetry showing regional response of tumor in Figure 7 to hyperoxic gas challenge. Sequential PO_2 maps were acquired for 6.5 min each, as shown in Figure 7. Mean values are shown for region close to tumor periphery (□) and for tumor center (Δ), together with mean values for whole tumor (♦). As expected, tumor periphery had higher baseline PO_2 and was far more responsive to hyperoxic gas breathing. Responses in both regions were rapid and reversible. It is apparent that global mean value was strongly biased by high values in peripheral region, emphasizing the importance of assessing regional variations.

in tissues longer, which should assist with long-term studies of oxygenation. HMDSO may also allow effective emulsification to permit intravenous or intraperitoneal administration.

In summary, both the ^{19}F MRI of C_6F_6 and the ^{1}H MRI of HMDSO approaches exploit the physical interaction of oxygen dissolving in nanodroplets of reporter and reveal absolute PO_2. Measurements are possible from anoxia to hyperbaric conditions, although the best precision is generally obtained below 10 mm Hg (*166,167*). This approach is conceptually different from the use of nitroimidazoles, which react chemically, leading to trapped adducts in hypoxic environments.

OTHER MR METHODS FOR IMAGING HYPOXIA

Three 2-nitroimidazoles chemically similar to those used for nuclear imaging have been labeled with multiple ^{19}F atoms for MR detection. ^{19}F NMR has a similar sensitivity to that of protons and has the advantage that there is essentiality no background signal. Thus, reporter molecules are readily identified. Introducing several equivalent atoms of ^{19}F can enhance the signal-to-noise ratio still further. This approach to investigate hypoxia has been reported by several groups as reviewed previously (*168–173*). However, the achievable signal-to-noise ratio is typically disappointing, usually requiring long data acquisition times and generally precluding imaging. This method is predicated on formation of reactive intermediates that can react with diverse cellular components trapping the reporter molecule. In terms of nuclear medicine approaches, this provides specific uptake, which may be compared with normal tissues to reveal hypoxia. For NMR detection, multiple NMR-active species may be generated, each with a different chemical shift and, hence, a broad line or poor signal-to-noise ratio. Moreover, adducts formed as macromolecules have restricted rotational freedom, causing severe line broadening and loss of signal attributed to these effects (*173*). Recently, Koutcher et al. (*174*) successfully demonstrated low resolution ^{19}F chemical shift imaging of trifluoroethoxy-MISO (TF-MISO) accumulation in rat breast and prostate tumors with a 1-h acquisition time after a dose of 75 mg/kg. Although the NMR approach avoids issues of radioactivity and limited shelf life, it requires administration of contrast agent at 400–1,600 mg/m^2 (*170*), as opposed to less than 15 μg per patient for ^{18}F-FMISO PET, and thus raises a concern about the toxicity and future clinical role of these reporter molecules.

Glycolysis, either aerobic or anaerobic, is often associated with tumors and is up-regulated by HIF-1 transcription. The end product of glycolysis is pyruvate and, in the presence of lactate dehydrogenase, LDH, which is also up-regulated by HIF-1, it catalyzes the quantitative formation of lactate, the same metabolite that can be measured by bioluminescence imaging. Mueller-Klieser has argued that determination of lactate in primary tumors may provide a useful classification for tumors that might lead to improved prognosis in clinical oncology (*175*), and a study involving patients with head and neck cancer showed that elevated tumor lactate predicted an increased risk of metastases (*176*). ^{1}H MRI provides a good method for measuring relative regional lactate levels (*177,178*) as a consequence of hypoxia but is not a direct measure of tissue PO_2.

ELECTRON SPIN RESONANCE

Reporter molecules have been developed for use with electron spin resonance (ESR or EPR), where the line width is highly sensitive to oxygen (*179*). Two primary approaches are used: direct injection of char crystals (*180,181*), phthalocyanine (*182*), or India ink (*183*) into tissue, most commonly tumors, although studies have also been reported of injection into brain, heart, and skeletal muscle; or intravenous infusion of water-soluble agents, which disseminate throughout the tumor vasculature (*184,185*). Measurements have traditionally used a spectroscopic approach to report PO_2 at single locations only after direct implantation of reporter into a single tissue location. Nonetheless, significant data have been achieved demonstrating hypoxia and reoxygenation with respect to irradiation, and the importance of timing successive radiation doses to coincide with reoxygenation (*186*). Char particles may be stable in tissue for weeks to years, allowing measurements of chronic changes in tissues accompanying tumor growth (*187*). Bratasz recently presented a dramatic increase in molecular sensitivity to oxygen by dissolving perchlorotriphenylmethyl triester radical in hexafluorobenzene, exploiting the very high O_2 solubility in HFB (*188*) as also exploited directly by ^{19}F MRI (*vide infra*) (*15*). The intravenous approach is noninvasive, but reporter molecules may predominately distribute in the well-perfused vasculature, potentially biasing measurements

toward the more well-oxygenated tumor regions. Progressive uptake and clearance of agents produce variable concentrations, and some agents degrade in tissue, requiring appropriate correction factors (*185*). Nonetheless, images of tumor oxygen distribution have been reported, including 3-dimensional representations (*184*), and Kuppusamy et al. have engineered high-speed electronics and algorithms for effective imaging. A recent innovation was predosing tumor cells with lithium octa-*N*-butoxy-naphtholcyanine, leading to uptake in culture. On subsequent implantation into mice, reporter molecules were retained, allowing PO_2 measurements over a period of many days (*189*). Spin radicals may also be applied to a combined ESR/NMR approach (OMRI) exploiting the Overhauser enhancement in the tissue water proton MRI signal that occurs by polarization transfer from free radicals after electromagnetic irradiation (*190*). ESR approaches show promise, but the current lack of appropriate instrumentation prevents widespread implementation.

OPTICAL IMAGING METHODS FOR MEASURING HYPOXIA

Although in vivo optical imaging methods do not yet have a role in human studies of hypoxia, they have played an important role in evaluating hypoxia imaging methods and they continue to have a role in evaluation of biopsy specimens. Many biochemical pathways are under oxygen regulation and can provide an elegant window on hypoxia, for example, induction of HIF-1 and transcription of Glut-1 and other secondary responses such as increased production of VEGF (*191*). Intrinsic radiation sensitivity may also be assessed using the comet assay described later. These assays do not involve in vivo imaging; each requires biopsy of the tumor. Other markers potentially associated with hypoxia may be found in the plasma or urine and have been correlated with clinical outcome (*192*).

Several antibodies have been prepared that react with different nitroimidazole derivatives so that tissue specimens from patients who have been injected with gram levels of these drugs can be stained and viewed by immunohistochemical methods or by cell-sorting techniques. Pimonidazole is the most well known of these probes for animal imaging, and it is commercially available as Hydroxyprobe-1 (Natural Pharmacia International) (*193*). In one animal study, pimonidazole (120 mg/kg intravenously) was used to test the validity of CA9 immunohistochemistry as a biomarker of hypoxia. The spatial distribution and fractional staining of both markers was similar, but CA9 did not respond to carbogen reoxygenation, whereas pimonidazole staining decreased when PO_2 returned to normal, establishing pimonidazole as the more accurate measure of hypoxia (*91*).

Pimonidazole binding has also been validated against the comet assay for measuring radiobiologic hypoxia (*194*). The comet assay is the name for a single-cell gel electrophoresis assay of single-strand breaks in DNA which Olive and Durand developed (*195*). Briefly, it involves exposing tumors to several grays of irradiation and then aspirating cells by fine needle and electrophoresing their alkaline lysate. DNA that has been broken by irradiation migrates faster, producing a comet-like tail that lengthens in direct proportion to the number of DNA breaks. This becomes a measure of radiobiologically significant hypoxia rather than simply a measure of PO_2 as generated by a polarographic electrode. In a study involving a fairly homogeneous population of 58 patients with head and neck cancer, electrode and comet fine-needle measurements in the same metastatic neck nodes found no correlation between the biophysical measurement and the radiobiologic measurement (*196*). This observation challenges the validity of the Eppendorf PO_2 histogram as a gold standard for clinically significant hypoxia.

Antibodies have been developed against the fluorinated 2-nitroimidazoles, EF3 and EF5. An immunohistochemical (IHC) assay for drug adducts of EF5 has been developed and applied to EMT6 spheroids to quantify radiobiologic hypoxia (*197*). The spheroids were incubated with EF5 in air-tight vessels with well-controlled PO_2 and they were subjected to irradiation under the same conditions. Cryosections of the spheroids exposed to EF5 were stained with a fluorescent anti-EF5 antibody to identify regions of hypoxia. There was limited staining of the periphery and no staining in the necrotic center but intense staining of the interior, much as in the autoradiograph of Figure 4. Reoxygenated spheroids showed no fluorescent staining, nor did hypoxic cells not exposed to EF5. Cells dissociated from spheroids were assayed by flow cytometry for calculation of the percentage of stained cells and used to verify the accuracy of the imaging technique. Cells containing the highest level of EF5 binding were also the cells with the most radiation resistance.

IHC methods are particularly useful for in vitro studies, including assay of human biopsy specimens. In a study of 28 human brain tumors, a comparison of EF5 binding and the PO_2 histogram revealed no statistical correlation between the 2 methods for detection of hypoxia although both methods indicated similar ranges for patients (*198*). Similar methods have been used to measure hypoxia in a series of patients with soft-tissue sarcomas. Patients were administered about 1.5 g of EF5 24–48 h before surgery, and biopsy specimens were stained as described previously. This pilot study supported the hypothesis that imaging hypoxia should provide an independent prognostic variable for outcome in high-grade sarcoma (*199*).

Tissue oxygenation can be measured directly using near-infrared oximetry to measure fractional oxygenation of Hb. This approach has been used intraoperatively in pigs to study regional myocardial oxygenation (*200*). The oxygenation levels were derived from spectroscopic images at 650 nm and the dHb levels at 1,050 nm. Light at these long wavelengths penetrates greater than 5 mm in tissues. Oxygenation in tissues correlated well with blood oxygen saturation levels. It is likely that this method will be more useful in the heart than in tumors because acute changes in

O_2 cause stress in the heart whereas tumors adapt to chronic hypoxia. This approach may be clinically useful in open-chest surgery. The nitroimidazoles have not proven useful for imaging myocardial hypoxia (*70,201,202*).

In a related method, sensors using quenching of the near-infrared fluorescent or phosphorescent lifetime of inorganic crystals by O_2 have been used for imaging PO_2 in cutaneous melanoma compared with adjacent skin that was clinically normal (*203*). The average difference between melanoma and normal tissue was 10 mm Hg, and the lowest average tumor PO_2 was 8 mm Hg, higher than in many solid tumors. It is not likely that this approach will have widespread clinical value, but it should find a role in small-animal studies and is finding an important role in cell biology (*204*) as new and more photostable chromophores are developed. The oxygen-quenching effect is rapidly reversible so that this assay is useful for observing rapid changes in oxygenation status, including reoxygenation. Furthermore, optical probes at different wavelengths can be used in the same cells to study different biochemical processes simultaneously, a feature that is particularly advantageous for optical systems and cannot be achieved with the other hypoxia imaging systems considered here.

Alternatively, surrogate markers of hypoxia have been measured. Bioluminescent imaging has been applied to flash-frozen tissue samples to detect, at the microscopic level, various characteristics of a tumor microenvironment, including metabolites such as glucose, ATP, and lactate. Walenta has provided a useful review of this technique (*205*). For example, bioluminescent imaging of lactate in specimens from patients with head and neck and uterine cervical cancer has established that a high level of lactate from glycolysis is associated with an increased rate of metastasis and poor outcome (*206*). Bioluminescent imaging provides an important tool for detailed examination of human biopsy material that will support translation of human observations to more detailed bench studies with small animals, cells, and tumor spheroids. For example, it is complementary to autoradiographic studies using PET radiopharmaceuticals as one way to validate the mechanistic interpretation of PET images.

Some elegant methods have been developed to directly measure HIF-1 activity by the introduction of transgenes with hypoxic response elements as promoter sequences coupled to reporter genes such as luciferase (*207,208*) or green fluorescent protein, GFP (*209*). A luciferase reporter gene under regulation of an HIF1-dependent promoter has been developed (*210*) for in vivo bioluminescent imaging. It is stable, expresses 100-fold increased luciferase in response to hypoxia, and has been used to evaluate the efficacy of a hypoxia-directed therapy in animals. Bioluminescence accompanying luciferase requires ATP and O_2, but reports suggest that even under exceedingly low PO_2, sufficient oxygen remains to reveal hypoxia. Another experiment used a retroviral vector with an HIF-1–inducible reporter gene for GFP (*211*). GFP synthesis is another energetic process that could be hindered under hypoxic conditions. These imaging tools are useful for studying the biology of hypoxia and mechanisms of response to experimental therapy but are unlikely to have a role in human imaging.

Imaging techniques based on optical contrast between O_2Hb and dHb can be combined with ultrasound detectors in a method called photoacoustic tomography, PAT. This technique overcomes the resolution limitations imposed by scattered photons in purely optical imaging. PAT retains intrinsic optical contrast but it uses an ultrasound (US) transducer to detect the resulting photoacoustic waves. A laser that emits visible light at a wavelength where O_2Hb and dHb absorb is pulsed for a short interval. Optical absorption in the laser-irradiation region generates photoacoustic waves proportional to the distribution of absorbing materials. The optically excited molecules produce a photoacoustic wave that can be detected by a very sensitive wide-bandwidth US transducer. This photoacoustic signal has the high spatial resolution and depth penetration characteristic of US, making it a practical method for human studies. PAT is a new technology but one with considerable promise. Although its role in human patients has not been evaluated, some early studies in animals show considerable promise (*212–214*).

CLINICAL ROLE OF HYPOXIA IMAGING

Identifying hypoxic tissue has therapeutic implications for multiple disease states including stroke, myocardial ischemia, and diabetes, as well as tumors (*78*). The selectivity of nitroimidazoles for hypoxic regions has been demonstrated in rat myocytes (*69*), the gerbil stroke model (*215,216*), pig and rat liver (*217–219*), and dog myocardium (*201,202*). In ischemic stroke, ^{18}F-FMISO was able to identify the areas of brain tissue to which a stroke extended (*220,221*). ^{18}F-FMISO has been evaluated for identifying chronic myocardial hypoxia as an alternative marker for viability (*52,222*). ^{18}F-FMISO distribution in the heart and other organs principally reflected the blood–tissue partition coefficient, except in liver and kidney, where the whole organ concentration was consistently higher than in blood.

The growing body of literature showing that hypoxia identified by imaging is predictive of poor survival in numerous cancer settings was reviewed along with each of the imaging agents. The next phase of studies evaluating the predictive value of hypoxia imaging in tumors needs to provide convincing data on the extent to which it is an independent predictive marker, in view of the many assays available to the oncologist. Furthermore, these trials needs to consider all therapeutic strategies, not just radiation therapy, in view of the mounting evidence that HIF-1 signals for upregulation of multiple factors that increase the survivability and metastatic spread of cancer cells (*22,35,36,40,43*).

The initial motivation for developing hypoxia imaging was the cure limitation imposed by hypoxia in response to radiation therapy. When all patients were treated with

various strategies designed to overcome the cure limitations of hypoxia, the results were disappointing (*23,24*). However, several groups have suggested that if only those patients with substantial levels of hypoxia were treated with escalating doses of ionizing radiation, a beneficial improvement in outcome might be achieved. Although it is unrealistic to increase the dose 3-fold, the value of the OER, a modest increase of 10 or 20 Gy might achieve significantly better local control. We are analyzing our ^{18}F-FMISO results in HNSCC (*91*) to test the hypothesis that primary regrowth occurs more frequently in sites that are ^{18}F-FMISO–positive and might potentially be treated with higher doses of radiation using image-guided treatment planning (*79,223*).

Because hypoxia is a common although not universal attribute of the tumor phenotype, efforts have been directed toward exploiting this characteristic in therapy. The hypoxic tumor phenotype could be turned to therapeutic advantage through drugs that are activated to cytotoxins only in the absence of normal PO_2. The first of these drugs to be tested in the clinic was tirapazamine (TPZ), originally referred to as SR4233 (*224*). The TPZ radical formed by electrons from 1 e^- reductases such as the cytochrome P450 reductases will abstract hydrogen atoms from DNA, producing both single- and double-strand breaks. Under aerobic conditions, O_2 can remove the additional electron before it gets close to a critical DNA target. TPZ and ionizing radiation act as complementary cytotoxins in that each one kills cells that are resistant to the other. TPZ also enhances the effectiveness of cisplatin, CIS (*225*). In a clinical trial of patients with HNSCC, those with hypoxic tumors (^{18}F-FMISO–positive) who received TPZ/CIS fared significantly better than the CIS/FU patients with hypoxic tumors with respect to the risk of locoregional failure (*81,226*). This outcome supports the efficacy of TPZ in the presence of hypoxic disease. Although normal-tissue toxicity has now stopped the clinical trials of TPZ, clinical trials of newer cytotoxins such as PR-104A have started. It is a soluble phosphate ester that is converted in vivo to the corresponding alcohol and then activated under hypoxic conditions to a cytotoxic nitrogen mustard prodrug (*227*). It will be important to assess whether these new agents reduce the quantity and distribution of hypoxic disease, something that should be feasible with hypoxia imaging.

CONCLUSION

Thus, molecular imaging of hypoxia has 2 clinically important roles, selecting a cohort of patients who might respond better to treatments designed to overcome the cure limitations of hypoxia and documenting through serial imaging that the treatment strategy reduced the extent of hypoxic disease. Molecular imaging has provided the oncology community with several options to choose from in assessing regional hypoxia. It takes molecular imaging beyond the role of tumor detection to the role of tumor characterization in support of personalized medicine.

ACKNOWLEDGMENTS

We gratefully acknowledge support from P01 CA42045 and S10 RR17229 from the National Institutes of Health; and support from the Simmons Cancer Center, Southwestern Cancer Imaging Program (SW-SAIRP U24 CA126608); and NIH BTRP facility P41-RR02584. We are grateful to Jesús Pacheco-Torres and Drs. Dawen Zhao, Vikram Kodibagkar, and Debu Saha for allowing us to present the unpublished observations shown in Fig. 7.

REFERENCES

1. Raichle ME. Behind the scenes of functional brain imaging: a historical and physiological perspective. *Proc Natl Acad Sci.* 1998;95:765–772.
2. Lu H, van Zijl PC. Experimental separation of intra and extravascular BOLD effects using multi-echo VASO and BOLD fMRI at 1.5T and 3.0T. *Magn Reson Med.* 2005;53:808–816.
3. Ter-Pogossian MM, Eichling JO, Davis DO, Welch MJ. The measure *in vivo* of regional oxygen utilization by means of oxyhemoglobin labeled with radioactive oxygen-15. *J Clin Invest.* 1970;49:381–391.
4. Ito M, Lammertsma AA, Wise RJS, et al. Measurement of regional cerebral blood flow and oxygen utilization in patients with cerebral tumours using ^{15}O and positron emission tomography: analytical techniques and preliminary results. *Neuroradiology.* 1982;23:63–74.
5. Derdeyn CP, Videen TO, Simmons NR, et al. Count-based PET method for predicting ischemic stroke in patients with symptomatic carotid arterial occlusion. *Radiology.* 1999;212:499–506.
6. Diringer MN, Aiyagari V, Zazulia AR, Videen TO, Powers WJ. Effect of hyperoxia on cerebral metabolic rate for oxygen measured using positron emission tomography in patients with acute severe head injury. *J Neurosurg.* 2007;106:526–529.
7. Vaupel P, Schlenger K, Knoop C, Hockel M. Oxygenation of human tumors: evaluation of tissue oxygen distribution in breast cancers by computerized O_2 tension measurements. *Cancer Res.* 1991;51:3316–3322.
8. Kavanagh MC, Sun A, Hu Q, Hill RP. Comparing techniques of measuring tumor hypoxia in different murine tumors: Eppendorf PO_2 histograph, [^{3}H]misonidazole binding and paired survival assay. *Radiat Res.* 1996;145:491–500.
9. Kim JG, Song Y, Zhao D, Constantinescu A, Mason RP, Liu H. Interplay of tumor vascular oxygenation and pO_2 in tumors using NIRS and needle electrode. In: Chance B, Alfano RR, Tromberg BJ, Tamura M, Sevick-Muraca EM, eds. *Optical Tomography and Spectroscopy of Tissue IV.* 2001;4250:429–436.
10. Mason RP, Hunjan S, Constantinescu A, et al. Tumor oximetry: comparison of ^{19}F MR EPI and electrodes. *Adv Exp Med Biol.* 2003:530:19–27.
11. Oxylite 2000 instrument. Oxford Optronix, Oxford, U.K. Available at: http://www.oxfordoptronix.com. Accessed May 12, 2008.
12. Gu Y, Bourke V, Kim JG, Constantinescu A, Mason RP, Liu H. Dynamic response of breast tumor oxygenation to hyperoxic respiratory challenge monitored with three oxygen-sensitive parameters. *Appl Opt.* 2003;42:2960–2967.
13. Zhao D, Constantinescu A, Hahn EW, Mason RP. Tumor oxygen dynamics with respect to growth and respiratory challenge: investigation of the Dunning prostate R3327-HI tumor. *Radiat Res.* 2001;156:510–520.
14. Zhao D, Jiang L, Hahn EW, Mason RP. Tumor physiological response to combretastatin A4 phosphate assessed by MRI. *Int J Radiat Oncol Biol Phys.* 2005;62:872–880.
15. Zhao D, Jiang L, Mason RP. Measuring changes in tumor oxygenation. *Methods Enzymol.* 2004;386:378–418.
16. Kim YR, Huang IJ, Lee SR, et al. Measurements of BOLD/CBV ratio show altered fMRI hemodynamics during stroke recovery in rats. *J Cereb Blood Flow Metab.* 2005;25:820–829.
17. Leontiev O, Buxton RB. Reproducibility of BOLD, perfusion, and $CMRO_2$ measurements with calibrated-BOLD fMRI. *Neuroimage.* 2007;35:175–184.
18. Jiang L, Zhao D, Constantinescu A, Mason RP. Comparison of BOLD contrast and Gd-DTPA dynamic contrast enhanced imaging in rat prostate tumor. *Magn Reson Med.* 2004;51:953–960.
19. Karczmar GS, Kuperman VY, River JN, Lewis MZ, Lipton MJ. Magnetic resonance measurement of response to hyperoxia differentiates tumors from normal tissue and may be sensitive to oxygen consumption. *Invest Radiol.* 1994;29:S161–S163.

20. O'Connor JPB, Jackson A, Buonaccorsi GA, et al. Organ-specific effects of oxygen and carbogen gas inhalation on tissue longitudinal relaxation times. *Magn Reson Med.* 2007;58:490–496.
21. Gray LH, Conger AD, Ebert M, et al. The concentration of oxygen dissolved in tissues at the time of irradiation as a factor in radiotherapy. *Br J Radiol.* 1953;26:638–648.
22. Brown JM, Wilson WR. Exploiting tumour hypoxia in cancer treatment. *Nat Rev Cancer.* 2004;4:437–447.
23. Overgaard J. Clinical evaluation of nitroimidazoles as modifiers of hypoxia in solid tumors. *Oncol Res.* 1994;6:509–518.
24. Overgaard J, Horsman MR. Modification of hypoxia-induced radioresistance in tumors by the use of oxygen and sensitizers. *Semin Radiat Oncol.* 1996;6:10–21.
25. Dische S, Saunders MI, Flockhart IR, Lee ME, Anderson P. Misonidazole: a drug for trial in radiotherapy and oncology. *Int J Radiat Oncol Biol Phys.* 1979;5:851–860.
26. Rasey JS, Koh WJ, Evans ML, et al. Quantifying regional hypoxia in human tumors with positron emission tomography of [^{18}F]fluoromisonidazole: a pretherapy study of 37 patients. *Int J Radiat Oncol Biol Phys.* 1996;36: 417–428.
27. Hockel M, Schlenger K, Knoop C, Vaupel P. Oxygenation of carcinomas of the uterine cervix: evaluation by computerized O_2 tension measurements. *Cancer Res.* 1991;51:6098–6102.
28. Brizel DM, Sibley GS, Prosnitz LR, Scher RL, Dewhirst MW. Tumor hypoxia adversely affects the prognosis of carcinoma of the head and neck. *Int J Radiat Oncol Biol Phys.* 1997;38:285–289.
29. Okunieff P, Dunphy EP, Hoeckel M, Terris DJ, Vaupel P. The role of oxygen tension distribution on the radiation response of human breast carcinoma. *Adv Exp Med Biol.* 1994;345:485–492.
30. Mueller-Klieser W, Schlenger KH, Walenta S, et al. Pathophysiological approaches to identifying tumor hypoxia in patients. *Radiother Oncol.* 1991; 20(suppl 1):21–28.
31. Hockel M, Knoop C, Schlenger K, et al. Intratumoral pO2 predicts survival in advanced cancer of the uterine cervix. *Radiother Oncol.* 1993;26:45–50.
32. Fyles AW, Milosevic M, Wong R, et al. Oxygenation predicts response and survival in patients with cervix cancer. *Radiother Oncol.* 1998;48:146–149.
33. Brizel DM, Scully SP, Harrelson JM, et al. Tumor oxygenation predicts for the likelihood of distant metastases in human soft tissue sarcoma. *Cancer Res.* 1996;56:941–943.
34. Wang GL, Jiang BH, Rue EA, Semenza GL. Hypoxia-inducible factor 1 is a basic-helix-loop-helix-PAS heterodimer regulated by cellular O_2 tension. *Proc Natl Acad Sci.* 1995;92:5510–5514.
35. Semenza GL. Targeting HIF-1 for cancer therapy. *Nat Rev Cancer.* 2003;3: 721–732.
36. Shaw RJ. Glucose metabolism and cancer. *Curr Opin Cell Biol.* 2006;18: 598–608.
37. Dang CV, Semenza GL. Oncogenic alterations of metabolism. *Trends Biochem Sci.* 1999;24:68–72.
38. Zelzer E, Levy Y, Kahana C, Shilo B-Z, Rubinstein M, Cohen B. Insulin induces transcription of target genes through the hypoxia-inducible factor HIF-1α/ARNT. *EMBO J.* 1998;17:5085–5094.
39. Lukashev D, Ohta A, Sitkovsky M. Hypoxia-dependent anti-inflammatory pathways in protection of cancerous tissues. *Cancer Metastasis Rev.* 2007;26: 273–279.
40. Chapman JD. Hypoxic sensitizers: implications for radiation therapy. *N Engl J Med.* 1979;301:1429–1432.
41. Chapman JD, Franko AJ, Sharplin J. A marker for hypoxic cells in tumours with potential clinical applicability. *Br J Cancer.* 1981;43:546–550.
42. Rasey JS, Martin GV, Krohn KA. Quantifying hypoxia with radiolabeled fluoromisonidazole: pre-clinical and clinical studies. In: Machulla H-J, ed. *The Imaging of Hypoxia.* Dordrecht, The Netherlands: Kluwer Academic Publishers; 1999:85–117.
43. Tatum JL, Kelloff GJ, Gilles RJ, et al. Hypoxia: importance in tumor biology, noninvasive measurement by imaging, and value of its measurement in the management of cancer therapy. *Int J Radiat Biol.* 2006;82:699–757.
44. Padhani AR, Krohn KA, Lewis JS, Alber M. Imaging oxygenation in human tumors. *Eur Radiol.* 2007;17:861–872.
45. Ballinger JR. Imaging hypoxia in tumors. *Semin Nucl Med.* 2001;31:321–329.
46. Lee ST, Scott AM. Hypoxia positron emission tomography imaging with ^{18}F-fluoromisonidazole. *Semin Nucl Med.* 2007;37:451–461.
47. Chapman JD. The detection and measurement of hypoxic cells in solid tumors. *Cancer.* 1984;54:2441–2449.
48. Blasberg R, Horowitz M, Strong J, et al. Regional measurements of [^{14}C]misonidazole distribution and blood flow in subcutaneous RT-9 experimental tumors. *Cancer Res.* 1985;45:1692–1699.
49. Rasey JS, Grunbaum Z, Magee S, et al. Characterization of radiolabeled fluoromisonidazole as a probe for hypoxic cells. *Radiat Res.* 1987;111:292–304.
50. Brown JM, Workman P. Partition coefficient as a guide to the development of radiosensitizers which are less toxic than misonidazole. *Radiat Res.* 1980;82: 171–190.
51. Grunbaum Z, Freauff SJ, Krohn KA, Wilbur DS, Magee S, Rasey JS. Synthesis and characterization of congeners of misonidazole for imaging hypoxia. *J Nucl Med.* 1987;28:68–75.
52. Martin GV, Caldwell JH, Graham MM, et al. Noninvasive detection of hypoxic myocardium using fluorine-18-fluoromisonidazole and positron emission tomography. *J Nucl Med.* 1992;33:2202–2208.
53. McClelland RA. Molecular interactions and biological effects of the products of reduction of nitroimidazoles. In: Adams GE, Breccia A, Fiedlen EN, Wardman P, eds. *NATO Advanced Research Workshop on Selective Activation of Drugs by Redox Processes.* New York, NY: Plenum Press; 1990: 125–136.
54. Prekeges JL, Rasey JS, Grunbaum Z, Krohn KA. Reduction of fluoromisonidazole, a new imaging agent for hypoxia. *Biochem Pharmacol.* 1991;42:2387–2395.
55. Zanzonico P, O'Donoghue J, Chapman DJ, et al. Iodine-124-labeled iodoazomycin-galactoside imaging of tumor hypoxia in mice with serial microPET scanning. *Eur J Nucl Med Mol Imaging.* 2004;31:117–128.
56. Biskupiak JE, Grierson JR, Rasey JS, Martin GV, Krohn KA. Synthesis of an (iodovinyl)misonidazole derivative for hypoxia imaging. *J Med Chem.* 1991; 34:2165–2168.
57. Nunn A, Linder K, Strauss HW. Nitroimidazoles and imaging hypoxia. *Eur J Nucl Med.* 1995;22:265–280.
58. Koch CJ, Evans SM. Non-invasive PET and SPECT imaging of tissue hypoxia using isotopically labeled 2-nitroimidazoles. *Adv Exp Med Biol.* 2003;510:285–292.
59. Raleigh J, Franko A, Kelly D, Trimble L, Allen P. Development of an in vivo ^{19}F MR method for measuring oxygen deficiency in tumors. *Magn Reson Med.* 1991;22:451–466.
60. Procissi D, Claus F, Burgman P, et al. *In vivo* ^{19}F magnetic resonance spectroscopy and chemical shift imaging of tri-fluoro-nitroimidazole as a potential hypoxia reporter in solid tumors. *Clin Cancer Res.* 2007;13:3738–3747.
61. Workman P. Pharmacokinetics of hypoxic cell radiosensitizers: a review. *Cancer Clin Trials.* 1980;3:237–251.
62. Dische S, Saunders MI, Anderson P, Stratford MR, Minchinton A. Clinical experience with nitroimidazoles as radiosensitizers. *Int J Radiat Oncol Biol Phys.* 1982;8:335–338.
63. Flockhart IR, Malcolm SL, Marten TR, Parkins CS, Ruane RJ, Troup D. Some aspects of the metabolism of misonidazole. *Br J Cancer Suppl.* 1978;37:264–267.
64. Raleigh JA, Koch CJ. Importance of thiols in the reductive binding of 2-nitroimidazoles to macromolecules. *Biochem Pharmacol.* 1990;40:2457–2464.
65. Saunders ME, Dische S, Anderson P, Flockhart IR. The neurotoxicity of misonidazole and its relationship to dose, half-life, and concentration in the serum. *Br J Cancer.* 1978;3:268–270.
66. Wiltshire CR, Workman P, Watson JV, Bleehan NM. Clinical studies with misonidazole. *Br J Cancer Suppl.* 1978;3:286–289.
67. Paget GE. Toxicity tests: a guide for clinicians. In: Heinrich AD, Cattell M, eds. *Clinical Testing of New Drugs.* New York, NY: Revere Publishing Co.; 1965.
68. Rasey JS, Grunbaum Z, Krohn KA, Nelson NJ, Chin L. Comparison of binding of ^{3}H-misonidazole and ^{14}C-misonidazole in multicell spheroids. *Radiat Res.* 1985;101:473–479.
69. Martin GV, Cerqueira MD, Caldwell JH, Rasey JS, Embree L, Krohn KA. Fluoromisonidazole: a metabolic marker of myocyte hypoxia. *Circ Res.* 1990;67:240–244.
70. Caldwell JH, Martin GV, Rasey JS, Krohn KA. Imaging myocardial hypoxia with positron emission tomography. In: Sidemen S, Beyar R, eds. *Imaging, Measurement, and Analysis of the Heart.* Washington, DC: Hemisphere Publishing Co.; 1991:323–333.
71. Jerabek PA, Patrick TB, Kilbourn MR, Dischino DD, Welch MJ. Synthesis and biodistribution of ^{18}F-labeled fluoronitroimidazoles: potential in vivo markers of hypoxic tissue. *Int J Rad Appl Instrum [A].* 1986;37:599–605.
72. Grierson JR, Link JM, Mathis CA, Rasey JS, Krohn KA. A radiosynthesis of fluorine-18 fluoromisonidazole. *J Nucl Med.* 1989;30:343–350.
73. Lim JL, Berridge MS. An efficient radiosynthesis of [^{18}F]fluoromisonidazole. *Appl Radiat Isot.* 1993;44:1085–1091.
74. NCI-CIP Web site. Available at: http://imaging.cancer.gov/programsandresources/Cancer-Tracer-Synthesis-Resources. Accessed October 25, 2007.

75. Adamsen TCH, Grierson JR, Krohn KA. A new synthesis of the labeling precursor for [^{18}F]-fluoromisonidazole. *J Labelled Comp Radiopharm.* 2005; 48:923–927.
76. Peterson LM, Muzi M, Adamsen TCH, et al. Enantiomeric form of FMISO is not critical for hypoxia imaging [abstract]. *J Labelled Comp Radiopharm.* 2007;50:S423.
77. Graham MM, Peterson LM, Link JM, et al. Fluorine-18-fluoromisonidazole radiation dosimetry in imaging studies. *J Nucl Med.* 1997;38:1631–1636.
78. Rajendran JG, Krohn KA. Imaging hypoxia and angiogenesis in tumors. *Radiol Clin North Am.* 2005:43:169–187.
79. Ling CC, Humm J, Larson S, et al. Towards multidimensional radiotherapy (MD-CRT): biological imaging and biological conformality. *Int J Radiat Oncol Biol Phys.* 2000;47:551–560.
80. Thorwarth D, Eschmann S-M, Paulsen F, et al. Hypoxia dose painting by numbers: a planning study. *Int J Radiat Oncol Biol Phys.* 2007;68:291–300.
81. Rischin D, Peters L, Hicks R, et al. Phase I trial of concurrent tirapazamine, cisplatin, and radiotherapy in patients with advanced head and neck cancer. *J Clin Oncol.* 2001;19:535–542.
82. Bruehlmeier M, Roelcke U, Schubiger PA, Ametamey SM. Assessment of hypoxia and perfusion in human brain tumors using PET with ^{18}F-fluoromisonidazole and ^{15}O-H_2O. *J Nucl Med.* 2004;45:1851–1859.
83. Rajendran JG, Wilson DC, Conrad EU, et al. ^{18}F-FMISO and ^{18}F-FDG PET imaging in soft tissue sarcomas: correlation of hypoxia, metabolism and VEGF expression. *Eur J Nucl Med Mol Imaging.* 2003;30:695–704.
84. Rajendran JG, Mankoff DA, O'Sullivan F, et al. Hypoxia and glucose metabolism in malignant tumors: evaluation by ^{18}F-fluoromisonidazole and ^{18}F-fluorodeoxyglucose positron emission tomography imaging. *Clin Cancer Res.* 2004;10:2245–2252.
85. Gagel B, Reinartz P, DeMartino E, et al. pO_2 polarography versus positron emission tomography ([^{18}F]fluoromisonidazole, [^{18}F]-2-fluoro-2′-deoxyglucose): an appraisal of radiotherapeutically relevant hypoxia. *Strahlenther Onkol.* 2004;180:616–622.
86. Cher LM, Murone C, Lawrentschuk N, et al. Correlation of hypoxic cell fraction and angiogenesis with glucose metabolic rate in gliomas using ^{18}F-fluoromisonidazole, ^{18}F-FDG PET, and immunohistochemical studies. *J Nucl Med.* 2006;47:410–418.
87. Cherk MH, Foo SS, Poon AMT, et al. Lack of correlation of hypoxic cell fraction and angiogenesis with glucose metabolic rate in non-small cell lung cancer assessed by ^{18}F-fluoromisonidazole and ^{18}F-FDG PET. *J Nucl Med.* 2006;47:1921–1926.
88. Grigsby PW, Malyapa RS, Higashikubo R, et al. Comparison of molecular markers of hypoxia and imaging with ^{60}Cu-ATSM in cancer of the uterine cervix. *Mol Imaging Biol.* 2007;9:278–283.
89. Eschmann SM, Paulsen F, Reimold M, et al. Prognostic impact of hypoxia imaging with ^{18}F-fluoromisonidazole PET in non-small cell lung cancer and head and neck cancer before radiotherapy. *J Nucl Med.* 2005;46:253–260.
90. Bentzen L, Keiding S, Nordsmark M, et al. Tumour oxygenation assessed by ^{18}F-fluoromisonidazole PET and polarographic needle electrodes in human soft tissue tumours. *Radiother Oncol.* 2003;67:339–344.
91. Rajendran JG, Schwartz DL, O'Sullivan J, et al. Tumor hypoxia imaging with [F-18]fluoromisonidazole position emission tomography in head and neck cancer. *Clin Cancer Res.* 2006;12:5435–5441.
92. Dubois L, Landuyt W, Haustermans K, et al. Evaluation of hypoxia in an experimental rat tumour model by [^{18}F]fluoromisonidazole PET and immunohistochemistry. *Br J Cancer.* 2004;91:1947–1954.
93. Shin KH, Diaz-Gonzalez JA, Russell J, et al. Detecting changes in tumor hypoxia with carbonic anhydrase IX and pimonidazole. *Cancer Biol Ther.* 2007;6:70–75.
94. Rasey JS, Hofstrand PD, Chin LK, Tewson TJ. Characterization of [^{18}F]fluoroetanidazole, a new radiopharmaceutical for detecting tumor hypoxia. *J Nucl Med.* 1999;40:1072–1079.
95. Lehtio K, Oikonen V, Nyman S, et al. Quantifying tumour hypoxia with fluorine-18 fluoroerythronitroimidazole ([^{18}F]FETNIM) and PET using the tumour to plasma ratio. *Eur J Nucl Med Mol Imaging.* 2003;30:101–108.
96. Gronroos T, Bentzen L, Marjamaki P, et al. Comparison of the biodistribution of two hypoxia markers [^{18}F]FETNIM and [^{18}F]FMISO in an experimental mammary carcinoma. *Eur J Nucl Med Mol Imaging.* 2004;31:513–520.
97. Yamamoto F, Oka H, Antoku S, Ichiya Y, Masuda K, Maeda M. Synthesis and characterization of lipophilic 1-^{18}F-fluoroalkyl-2-nitroimidazoles for imaging hypoxia. *Biol Pharm Bull.* 1999;22:590–597.
98. Sorger D, Patt M, Kumar P, et al. ^{18}F-fluoroazomycinarabinofuranoside (^{18}FAZA) and ^{18}F-fluoromisonidazole (^{18}FMISO): a comparative study of their selective uptake in hypoxic cells and PET imaging in experimental rat tumors. *Nucl Med Biol.* 2003;30:317–326.
99. Souvatzoglou M, Grosu AL, Roper B, et al. Tumour hypoxia imaging with [^{18}F]FAZA PET in head and neck cancer patients: a pilot study. *Eur J Nucl Med Mol Imaging.* 2007;34:1566–1575.
100. Piert M, Machulla H-J, Picchio M, et al. Hypoxia-specific tumor imaging with ^{18}F-fluoroazomycin arabinoside. *J Nucl Med.* 2005;46:106–113.
101. Zanzonico P, O'Donoghue J, Chapman JD, et al. Iodine-124-labeled iodoazomycin-galactoside imaging of tumor hypoxia in mice with serial microPET scanning. *Eur J Nucl Med Mol Imaging.* 2004;31:117–128.
102. Barthel H, Wilson H, Collingridge DR, et al. *In vivo* evaluation of [^{18}F]fluoroetanidazole as a new marker for imaging tumour hypoxia with positron emission tomography. *Br J Cancer.* 2004;90:2232–2242.
103. Evans SM, Kachur AV, Shiue C-Y, et al. Noninvasive detection of tumor hypoxia using the 2-nitroimidazole [^{18}F]EF1. *J Nucl Med.* 2000;41:327–336.
104. Christian N, Bol A, De Bast M, et al. Determination of tumour hypoxia with the PET tracer [^{18}F]EF3: improvement of the tumour-to-background ratio in a mouse tumour model. *Eur J Nucl Med Mol Imaging.* 2007;34:1348–1354.
105. Ziemer LS, Evans SM, Kachur AV, et al. Noninvasive imaging of tumor hypoxia in rats using the 2-nitroimidazole ^{18}F-EF5. *Eur J Nucl Med.* 2003;30: 259–266.
106. Dolbier WR Jr, Li AR, Koch CJ, Shiue CY, Kachur AV. [F-18]-EF5, a marker for PET detection of hypoxia: synthesis of precursor and a new fluorination procedure. *Appl Radiat Isot.* 2001;43:73–80.
107. Fujibayshi Y, Taniuchi H, Yonekura Y, Ohtani H, Konishi J, Yokoyama A. Copper-62-ATSM: a new hypoxia imaging agent with high membrane permeability and low redox potential. *J Nucl Med.* 1997;38:1155–1160.
108. Vavere AL, Lewis JS. Cu-ATSM: a radiopharmaceutical for the PET imaging of hypoxia. *Dalton Trans.* 2007;43:4893–4902.
109. Green MA, Mathias CJ, Welch MJ, et al. Copper-62-labeled pyruvaldehyde bis(N^4-methylthiosemicarbazonato)copper(II): synthesis and evaluation as a positron emission tomography tracer for cerebral and myocardial perfusion. *J Nucl Med.* 1990;31:1989–1996.
110. Burgman P, O'Donoghue JA, Lewis JS, Welch MJ, Humm JL, Ling CC. Cell line-dependent differences in uptake and retention of the hypoxia-selective nuclear imaging agent Cu-ATSM. *Nucl Med Biol.* 2005;32:623–630.
111. O'Donoghue JA, Zanzonico P, Pugachev A, et al. Assessment of regional tumor hypoxia using ^{18}F-fluoromisonidazole and ^{64}Cu(II)-diacetyl-bis(N4-methylthiosemicarbazone) positron emission tomography: comparative study featuring microPET imaging, PO_2 probe measurement, autoradiography, and fluorescent microscopy in the R3327-AT and FaDu rat tumor models. *Int J Radiat Oncol Biol Phys.* 2005;61:1493–1502.
112. Matsumoto K-I, Szajek L, Krishna MC, et al. The influence of tumor oxygenation on hypoxia imaging in murine squamous cell carcinoma using [^{64}Cu]Cu-ATSM or [^{18}F]fluoromisonidazole positron emission tomography. *Int J Oncol.* 2007;30:873–881.
113. Lewis JS, McCarthy DW, McCarthy TJ, Fujibayashi Y, Welch MJ. Evaluation of ^{64}Cu-ATSM in vitro and in vivo in a hypoxic tumor model. *J Nucl Med.* 1999;40:177–183.
114. Lewis JS, Sharp TL, Laforest R, Fujibayashi Y, Welch MJ. Tumor uptake of copper-diacetyl-bis(N(4)-methylthiosemicarbazone): effect of changes in tissue oxygenation. *J Nucl Med.* 2001;42:655–661.
115. Lewis JS, Herrero P, Sharp TL, et al. Delineation of hypoxia in canine myocardium using PET and copper(II)-diacetyl-bis(N(4)-methylthiosemicarbazone). *J Nucl Med.* 2002;43:1557–1569.
116. Dehdashti F, Mintun MA, Lewis JS, et al. In vivo assessment of tumor hypoxia in lung cancer with ^{60}Cu-ATSM. *Eur J Nucl Med Mol Imaging.* 2003;30: 844–850.
117. Grigsby PW, Malyapa RS, Higashikubo R, et al. Comparison of molecular markers of hypoxia and imaging with ^{60}Cu-ATSM in cancer of the uterine cervix. *Mol Imaging Biol.* 2007;9:278–283.
118. Dehdashti F, Grigsby PW, Mintun MA, Lewis JS, Siegel BA, Welch MJ. Assessing tumor hypoxia in cervical cancer by positron emission tomography with ^{60}Cu-ATSM: relationship to therapeutic response—a preliminary report. *Int J Radiat Oncol Biol Phys.* 2003;55:1233–1238.
119. Nield LE, Qi XL, Valsangiacomo ER, et al. In vivo MRI measurement of blood oxygen saturation in children with congenital heart disease. *Pediatr Radiol.* 2005;35:179–185.
120. Li K, Wright GA, Pelc LR, et al. Oxygen saturation of blood in the superior mesenteric vein: in vivo verification of MR imaging measurements in a canine model. *Radiology.* 1995;194:321–325.
121. Stainsby JA, Wright GA. Partial volume effects on vascular T2 measurements. *Magn Reson Med.* 1998;40:494–499.
122. Howe FA, Robinson SP, Rodrigues LM, Griffiths JR. Flow and oxygenation dependent (FLOOD) contrast MR imaging to monitor the response of rat tumors to carbogen breathing. *Magn Reson Imaging.* 1999;17:1307–1318.

123. Howe FA, Robinson SP, McIntyre DJ, Stubbs M, Griffiths JR. Issues in flow and oxygenation dependent contrast (FLOOD) imaging of tumours. *NMR Biomed.* 2001;14:497–506.
124. Al-Hallaq HA, River JN, Zamora M, Oikawa H, Karczma GS. Correlation of magnetic resonance and oxygen microelectrode measurements of carbogen-induced changes in tumor oxygenation. *Int J Radiat Oncol Biol Phys.* 1998; 41:151–159.
125. Baudelet C, Gallez B. How does blood oxygen level-dependent (BOLD) contrast correlate with oxygen partial pressure (pO_2) inside tumors? *Magn Reson Med.* 2002;48:980–986.
126. Denekamp J, Fowler JF. ARCON: current status—summary of a workshop on preclinical and clinical studies. *Acta Oncol.* 1997;36:517–525.
127. Kaanders JH, Pop LA, Marres HA, et al. Accelerated radiotherapy with carbogen and nicotinamide (ARCON) for laryngeal cancer. *Radiother Oncol.* 1998;48:115–122.
128. Rijpkema M, Kaanders JH, Joosten FB, van der Kogel AJ, Heerschap A. Effects of breathing a hyperoxic hypercapnic gas mixture on blood oxygenation and vascularity of head-and-neck tumors as measured by magnetic resonance imaging. *Int J Radiat Oncol Biol Phys.* 2002;53:1185–1191.
129. Xia M, Kodibagkar V, Liu H, Mason RP. Tumour oxygen dynamics measured simultaneously by near-infrared spectroscopy and ^{19}F magnetic resonance imaging in rats. *Phys Med Biol.* 2006;51:45–60.
130. Hunjan S, Mason RP, Constantinescu A, Peschke P, Hahn EW, Antich PP. Regional tumor oximetry: ^{19}F NMR spectroscopy of hexafluorobenzene. *Int J Radiat Oncol Biol Phys.* 1998;40:161–171.
131. Zhao D, Constantinescu A, Jiang L, Hahn EW, Mason RP. Prognostic Radiology: quantitative assessment of tumor oxygen dynamics by MRI. *Am J Clin Oncol.* 2001;24:462–466.
132. Mason RP, Hunjan S, Constantinescu A, et al. Tumor oximetry: comparison of ^{19}F MR EPI and electrodes. *Adv Exp Med Biol.* 2003;530:19–27.
133. Zhao D, Constantinescu C, Hahn EW, Mason RP. Differential oxygen dynamics in two diverse Dunning prostate R3327 rat tumor sublines (MAT-Lu and HI) with respect to growth and respiratory challenge. *Int J Radiat Oncol Biol Phys.* 2002;53:744–756.
134. Neeman M, Dafni H, Bukhari O, Braun RD, Dewhirst MW. In vivo BOLD contrast MRI mapping of subcutaneous vascular function and maturation: validation by intravital microscopy. *Magn Reson Med.* 2001;45:887–898.
135. Hsu YY, Chang CN, Jung SM, et al. Blood oxygenation level-dependent MRI of cerebral gliomas during breath holding. *J Magn Reson Imaging.* 2004;19: 160–167.
136. Rauscher A, Sedlacik J, Barth M, Haacke EM, Reichenbach JR. Noninvasive assessment of vascular architecture and function during modulated blood oxygenation using susceptibility weighted magnetic resonance imaging. *Magn Reson Med.* 2005;54:87–95.
137. Hoskin PJ, Carnell DM, Taylor NJ, et al. Hypoxia in prostate cancer: correlation of BOLD-MRI with pimonidazole immunohistochemistry—initial observations. *Int J Radiat Oncol Biol Phys.* 2007;68:1065–1071.
138. Taylor NJ, Baddeley H, Goodchild KA, et al. BOLD MRI of human tumor oxygenation during carbogen breathing. *J Magn Reson Imaging.* 2001;14:156–163.
139. Jiang L, McColl R, Weatherall P, Tripathy D, Mason RP. Blood oxygenation level dependent (BOLD) contrast MRI for early evaluation of breast cancer chemotherapy. *Breast Cancer Res Treat.* 2005;94:S257–S258.
140. Mason RP, Shukla HP, Antich PP. *In vivo* oxygen tension and temperature: simultaneous determination using ^{19}F NMR spectroscopy of perfluorocarbon. *Magn Reson Med.* 1993;29:296–302.
141. Thomas SR, Pratt RG, Millard RW, et al. Evaluation of the influence of the aqueous phase bioconstituent environment on the F-19 T1 of perfluorocarbon blood substitute emulsions. *J Magn Reson Imaging.* 1994;4:631–635.
142. Thomas SR. The biomedical applications of fluorine-19 NMR. In: Partain CL, Price RR, Patton JA, Kulkarni MV, James AEJ, eds. *Magnetic Resonance Imaging.* Vol. 2. London, U.K.: WB Saunders Co.; 1988;1536–1552.
143. Thomas SR, Pratt RG, Millard RW, et al. In vivo PO_2 imaging in the porcine model with perfluorocarbon F-19 NMR at low field. *Magn Reson Imaging.* 1996;14:103–114.
144. Higuchi T, Naruse S, Horikawa Y, Hirakawa K, Tanaka C. *In vivo* measurement of the partial pressure of oxygen in brain tissue using ^{19}F NMR. In: Opella SJ, ed. *7th SMRM.* Burlington, MA: Elsevier Inc.;1988:435.
145. Barker BR, Mason RP, Bansal N, Peshock RM. Oxygen tension mapping by ^{19}F echo-planar MR imaging of sequestered perfluorocarbon. *J Magn Reson Imaging.* 1994;4:595–602.
146. Holland SK, Kennan RP, Schaub MM, D'Angelo MJ, Gore JC. Imaging oxygen tension in liver and spleen by ^{19}F NMR. *Magn Reson Med.* 1993;29: 446–458.
147. Tran HT, Guo QZ, Schumacher DJ, Burton RB, Mattrey RF. ^{19}F chemical shift imaging technique to measure intracellular pO2 in vivo using perflubron. *Acad Radiol.* 1995;2:756–761.
148. Mason RP, Jeffrey FM, Malloy CR, Babcock EE, Antich PP. A noninvasive assessment of myocardial oxygen tension: ^{19}F NMR spectroscopy of sequestered perfluorocarbon emulsion. *Magn Reson Med.* 1992;27:310–317.
149. Rosenblum WI, Hadfield MG, Martinez AJ, Schatzki P. Alterations of liver and spleen following intravenous infusion of fluorocarbon emulsions. *Arch Pathol Lab Med.* 1976;100:213–217.
150. Mason RP, Antich PP, Babcock EE, Constantinescu A, Peschke P, Hahn EW. Non-invasive determination of tumor oxygen tension and local variation with growth. *Int J Radiat Oncol Biol Phys.* 1994;29:95–103.
151. Hunjan S, Zhao D, Constantinescu A, Hahn EW, Antich PP, Mason RP. Tumor oximetry: demonstration of an enhanced dynamic mapping procedure using fluorine-19 echo planar magnetic resonance imaging in the Dunning prostate R3327-AT1 rat tumor. *Int J Radiat Oncol Biol Phys.* 2001;49:1097–1108.
152. Song Y, Constantinescu A, Mason RP. Dynamic breast tumor oximetry: the development of prognostic radiology. *Technol Cancer Res Treat.* 2002;1:471–478.
153. Dardzinski BJ, Sotak CH. Rapid tissue oxygen tension mapping using ^{19}F inversion-recovery echo-planar imaging of perfluoro-15-crown-5-ether. *Magn Reson Med.* 1994;32:88–97.
154. van der Sanden BP, Heerschap A, Simonetti AW, et al. Characterization and validation of noninvasive oxygen tension measurements in human glioma xenografts by ^{19}F-MR relaxometry. *Int J Radiat Oncol Biol Phys.* 1999;44: 649–658.
155. Baldwin NJ, Ng TC. Oxygenation and metabolic status of KHT tumors as measured simultaneously by ^{19}F magnetic resonance imaging and ^{31}P magnetic resonance spectroscopy. *Magn Reson Imaging.* 1996;14:541–551.
156. Mason RP, Rodbumrung W, Antich PP. Hexafluorobenzene: a sensitive ^{19}F NMR indicator of tumor oxygenation. *NMR Biomed.* 1996;9:125–134.
157. Mason RP, Constantinescu A, Hunjan S, et al. Regional tumor oxygenation and measurement of dynamic changes. *Radiat Res.* 1999;152:239–249.
158. Bourke VA. *Dynamic Interrogation of the Tumor Microenvironment in Response to Respiratory Challenge, Radiation Therapy, and Pharmacologic Intervention* [dissertation]. Dallas, TX: UT Southwestern; 2005.
159. Zhao D, Ran S, Constantinescu A, Hahn EW, Mason RP. Tumor oxygen dynamics: correlation of in vivo MRI with histological findings. *Neoplasia.* 2003;5:308–318.
160. Zhao D, Constantinescu A, Chang CH, Hahn EW, Mason RP. Correlation of tumor oxygen dynamics with radiation response of the Dunning prostate R3327-HI tumor. *Radiat Res.* 2003;159:621–631.
161. Bourke VA, Zhao D, Gilio J, et al. Correlation of radiation response with tumor oxygenation in the Dunning prostate R3327-AT1 tumor. *Int J Radiat Oncol Biol Phys.* 2007;67:1179–1186.
162. Courtney KD, Andrews JE. Teratogenic evaluation and fetal deposition of hexabromobenzene (HBB) and hexafluorobenzene (HFB) in CD-1 mice. *J Environ Sci Health B.* 1984;19:83–94.
163. Hall LW, Jackson SRK, Massey GM. Hexafluorobenzene in veterinary anaesthesia. In: Arias A, Llaurado R, Nalda MA, et al., eds. *Recent Progress in Anaesthesiology and Resuscitation.* Oxford, U.K.: Excerpta Medica; 1975: 201–204.
164. Mortelmans KM, Simmon VF. *"In vitro"* microbiological mutagenicity assays of eight fluorocarbon taggant samples. *Gov Rep Announce Index (US).* 1981; 81:2555–2587.
165. Kodibagkar VD, Cui W, Merritt ME, Mason RP. Novel ^{1}H NMR approach to quantitative tissue oximetry using hexamethyldisiloxane. *Magn Reson Med.* 2006;55:743–748.
166. Delpuech J-J, Hamza MA, Serratice G, Stébé M-J. Fluorocarbons as oxygen carriers: an NMR study of oxygen solutions in hexafluorobenzene. *J Chem Phys.* 1979;70:2680–2687.
167. Hamza MA, Serratice G, Stebe M-J, Delpuech J-J. Solute-solvent interactions in perfluorocarbon solutions of oxygen: an NMR study. *J Am Chem Soc.* 1981;103:3733–3738.
168. Robinson SP, Griffiths JR. Current issues in the utility of ^{19}F nuclear magnetic resonance methodologies for the assessment of tumour hypoxia. *Philos Trans R Soc Lond B Biol Sci.* 2004;359:987–996.
169. Cline JM, Rosner GL, Raleigh JA, Thrall DE. Quantification of CCI-103F labeling heterogeneity in canine solid tumors. *Int J Radiat Oncol Biol Phys.* 1997;37:655–662.
170. Seddon BM, Payne GS, Simmons L, et al. A phase I study of SR-4554 via intravenous administration for noninvasive investigation of tumor hypoxia by magnetic resonance spectroscopy in patients with malignancy. *Clin Cancer Res.* 2003;9:5101–5112.

171. Li SJ, Jin GY, Moulder JE. Prediction of tumor radiosensitivity by hexafluoromisonidazole retention monitored by [H-1]/[F-19] magnetic-resonance spectroscopy. *Cancer Commun.* 1991;3:133–139.
172. Aboagye EO, Maxwell RJ, Horsman MR, et al. The relationship between tumour oxygenation determined by oxygen electrode measurements and magnetic resonance spectroscopy of the fluorinated 2-nitroimidazole SR-4554. *Br J Cancer.* 1998;77:65–70.
173. Salmon HW, Siemann DW. Utility of ^{19}F MRS detection of the hypoxic cell marker EF5 to assess cellular hypoxia in solid tumors. *Radiother Oncol.* 2004;73:359–366.
174. Procissi D, Claus F, Burgman P, et al. In vivo F-19 magnetic resonance spectroscopy and chemical shift imaging of tri-fluoro-nitroimidazole as a potential hypoxia reporter in solid tumors. *Clin Cancer Res.* 2007;13:3738–3747.
175. Walenta S, Schroeder T, Mueller-Klieser W. Lactate in solid malignant tumors: potential basis of a metabolic classification in clinical oncology. *Curr Med Chem.* 2004;11:2195–2204.
176. Brizel DM, Schoeder T, Scher R, et al. Elevated tumor lactate concentrations predict for an increased risk of metastases in head-and-neck cancer. *Int J Radiat Oncol Biol Phys.* 2001;51:349–353.
177. Adalsteinsson E, Spielman DM, Pauly JM, Terris DJ, Sommer G, Macovski A. Feasibility study of lactate imaging of head and neck tumors. *NMR Biomed.* 1998;11:360–369.
178. Tarnawski R, Sokol M, Pieniazek P, et al. ^{1}H-MRS in vivo predicts the early treatment outcome of postoperative radiotherapy for malignant gliomas. *Int J Radiat Oncol Biol Phys.* 2002;52:1271–1276.
179. Gallez B, Baudelet C, Jordan BF. Assessment of tumor oxygenation by electron paramagnetic resonance: principles and applications. *NMR Biomed.* 2004;17:240–262.
180. Vahidi N, Clarkson RB, Liu KJ, Norby SW, Wu M, Swartz HM. In vivo and in vitro EPR oximetry with fusinite: a new coal-derived, particulate EPR probe. *Magn Reson Med.* 1994;31:139–146.
181. He J, Beghein N, Ceroke P, Clarkson RB, Swartz HM, Gallez B. Development of biocompatible oxygen-permeable films holding paramagnetic carbon particles: evaluation of their performance and stability in EPR oximetry. *Magn Reson Med.* 2001;46:610–614.
182. Glockner JF, Swartz HM. In vivo oximetry using two novel probes: fusinite and lithium phthalocyanine. In: Erdmann W, Bruley DF, eds. *Oxygen Transport to Tissue XIV.* New York, NY: Plenum Press; 1992:229–234.
183. Goda F, Liu KJ, Walczak T, O'Hara JA, Jiang J, Swartz HM. *In vivo* oximetry using EPR and India ink. *Magn Reson Med.* 1995;33:237–245.
184. Elas M, Williams BB, Parasca A, et al. Quantitative tumor oxymetric images from 4D electron paramagnetic resonance imaging (EPRI): methodology and comparison with blood oxygen level-dependent (BOLD) MRI. *Magn Reson Med.* 2003;49:682–691.
185. Kuppusamy P, Afework R, Shankar RA, et al. *In vivo* electron paramagnetic resonance imaging of tumor heterogeneity and oxygenation in a murine model. *Cancer Res.* 1998;58:1562–1568.
186. O'Hara JA, Goda F, Demidenko E, Swartz HM. Effect on regrowth delay in a murine tumor of scheduling split-dose irradiation based on direct PO_2 measurements by electron paramagnetic resonance oximetry. *Radiat Res.* 1998;150:549–556.
187. Swartz HM. Measuring real levels of oxygen in vivo: opportunities and challenges. *Biochem Soc Trans.* 2002;30:248–252.
188. Bratasz A, Kulkarni AC, Kuppusamy P. A highly sensitive biocompatible spin probe for imaging of oxygen concentration in tissues. *Biophys J.* 2007;92:2918–2925.
189. Bratasz A, Pandian RP, Deng Y, et al. In vivo imaging of changes in tumor oxygenation during growth and after treatment. *Magn Reson Med.* 2007;57:950–959.
190. Krishna MC, English S, Yamada K, et al. Overhauser enhanced magnetic resonance imaging for tumor oximetry: coregistration of tumor anatomy and tissue oxygen concentration. *Proc Natl Acad Sci USA.* 2002;99:2216–2221.
191. Knowles HJ, Harris AL. Hypoxia and oxidative stress in breast cancer: hypoxia and tumourigenesis. *Breast Cancer Res.* 2001;3:318–322.
192. Le QT, Sutphin PD, Raychaudhuri S, et al. Identification of osteopontin as a prognostic plasma marker for head and neck squamous cell carcinomas. *Clin Cancer Res.* 2003;9:59–67.
193. Chemicon T. Available at: http://www.chemicon.com. Accessed October 25, 2007.
194. Olive PL, Durand RE, Raleigh JA, Luo D, Aquino-Parsons C. Comparison between the comet assay and pimonidazole binding for measuring tumour hypoxia. *Br J Cancer.* 2000;83:1525–1531.
195. Olive PL, Durand RE. Detection of hypoxic cells in a murine tumor with the use of the comet assay. *J Natl Cancer Inst.* 1992;84:707–711.
196. Le QT, Kovacs MS, Dorie JM, et al. Comparison of the comet assay and the oxygen microelectrode for measuring tumor oxygenation in head-and-neck cancer patients. *Int J Radiat Oncol Biol Phys.* 2003;56:375–383.
197. Woods ML, Koch CJ, Lord EM. Detection of individual hypoxic cells in multicellular spheroids by flow cytometry using the 2-nitroimidazole, EF5, and monoclonal antibodies. *Int J Radiat Oncol Biol Phys.* 1996;34:93–101.
198. Evans SM, Judy KD, Dunphy I, et al. Comparative measurements of hypoxia in human brain tumors using needle electrodes and EF5 binding. *Cancer Res.* 2004;64:1886–1892.
199. Evans SM, Fraker D, Hahn SM, et al. EF5 binding and clinical outcome in human soft tissue sarcomas. *Int J Radiat Oncol Biol Phys.* 2006;64:922–927.
200. Nighswander-Rempel SP, Kupriyanov VV, Shaw RA. Regional cardiac tissue oxygenation as a function of blood flow and pO_2: a near-infrared spectroscopic imaging study. *J Biomed Optics.* 2006;11:054004-1-10.
201. Caldwell JH, Revenaugh JR, Martin GV, et al. Comparison of fluorine-18-fluorodeoxyglucose and tritiated fluoromisonidazole uptake during low-flow ischemia. *J Nucl Med.* 1995;36:1633–1638.
202. Shelton ME, Dence CS, Hwang DR, et al. In vivo delineation of myocardial hypoxia during coronary occlusion using fluorine-18 fluoromisonidazole and positron emission tomography: a potential approach for identification of jeopardized myocardium. *J Am Coll Cardiol.* 1990;16:477–485.
203. Hartmann P, Mirtolouei R, Untersberger S, et al. Non-invasive imaging of tissue PO_2 in malignant melanoma of the skin. *Melanoma Res.* 2006;16:479–486.
204. O'Riordan TC, Fitzgerald K, Ponomarev GV, et al. Sensing intracellular oxygen using near-infrared phosphorescent probes and live-cell fluorescence imaging. *Am J Physiol Regul Integr Comp Physiol.* 2007;292:R1613–R1620.
205. Walenta S, Schroeder T, Mueller-Klieser W. Metabolic mapping with bioluminescence: basic and clinical relevance. *Biomol Eng.* 2002;18:249–262.
206. Walenta S, Wetterling M, Lehrke M, et al. High lactate levels predict likelihood of metastases, tumor recurrence, and restricted patient survival in human cervical cancers. *Cancer Res.* 2006;60:916–921.
207. Shibata T, Giaccia AJ, Brown JM. Development of a hypoxia-responsive vector for tumor-specific gene therapy. *Gene Ther.* 2000;7:493–498.
208. Payen E, Bettan M, Henri A, et al. Oxygen tension and a pharmacological switch in the regulation of transgene expression for gene therapy. *J Gene Med.* 2001;3:498–504.
209. Vordermark D, Shibata T, Brown JM. Green fluorescent protein is a suitable reporter of tumor hypoxia despite an oxygen requirement for chromophore formation. *Neoplasia.* 2001;3:527–534.
210. Harada H, Kizaka-Kondoh S, Hiraoka M. Optical imaging of tumor hypoxia and evaluation of efficacy of a hypoxia-targeting drug in living animals. *Mol Imaging.* 2005;4:182–193.
211. Serganova I, Doubrovin M, Vider J, et al. Molecular imaging of temporal dynamics and spatial heterogeneity of hypoxia-inducible factor-1 signal transduction activity in tumors in living mice. *Cancer Res.* 2004;64:6101–6108.
212. Wang X, Xie X, Ku G, Wang LV, Stoica G. Noninvasive imaging of hemoglobin concentration and oxygenation in the rat brain using high-resolution photoacoustic tomography. *J Biomed Opt.* 2006;11(2):024015 (9 pages).
213. Lungu GF, Li ML, Xie X, Wang LV, Stoica G. In vivo imaging and characterization of hypoxia-induced neovascularization and tumor invasion. *Int J Oncol.* 2007;30:45–54.
214. Kim G, Huang SW, Day KC, et al. Indocyanine-green-embedded PEBBLEs as a contrast agent for photoacoustic imaging. *J Biomed Opt.* 2007;12:044020.
215. Rasey JS, Hoffman JM, Spence AM. Hypoxia mediated binding of misonidazole in non-malignant tissue. *Int J Radiat Oncol Biol Phys.* 1986;12:1255–1258.
216. Hoffman JM, Rasey JS, Spence AM, et al. Binding of the hypoxia tracer [^{3}H]misonidazole in cerebral ischemia. *Stroke.* 1987;18:168–176.
217. Smith BR, Born JL. Metabolism and excretion of [^{3}H]misonidazole by hypoxic rat liver. *Int J Radiat Oncol Biol Phys.* 1984;10:1365–1370.
218. Piert M, Machulla H, Becker G, et al. Introducing fluorine-18 fluoromisonidazole positron emission tomography for the localisation and quantification of pig liver hypoxia. *Eur J Nucl Med.* 1999;26:95–109.
219. Piert M, Machulla HJ, Becker G, et al. Dependency of the [^{18}F]fluoromisonidazole uptake on oxygen delivery and tissue oxygenation in the porcine liver. *Nucl Med Biol.* 2000;27:693–700.
220. Read SJ, Hirano T, Abbott DF, et al. The fate of hypoxic tissue on ^{18}F-fluoromisonidazole positron emission tomography after ischemic stroke. *Ann Neurol.* 2000;48:228–235.
221. Markus R, Reutens DC, Kazui S, et al. Topography and temporal evolution of hypoxic viable tissue identified by ^{18}F-fluoromisonidazole positron

emission tomography in humans after ischemic stroke. *Stroke.* 2003;34: 2646–2652.

222. Martin GV, Caldwell JH, Rasey JS, Grunbaum Z, Cerqueira M, Krohn KA. Enhanced binding of the hypoxic cell marker [^{3}H]fluoromisonidazole in ischemic myocardium. *J Nucl Med.* 1989;30:194–201.
223. Rajendran JG, Hendrickson KR, Spence AM, Muzi M, Krohn KA, Mankoff DA. Hypoxia imaging-directed radiation treatment planning. *Eur J Nucl Med Mol Imaging.* 2006;33(suppl 1):44–53.
224. Zeman EM, Brown JM, Lemmon MJ, Hirst VK, Lee WW. SR-4233: a new bioreductive agent with high selective toxicity for hypoxic mammalian cells. *Int J Radiat Oncol Biol Phys.* 1986;12:1239–1242.
225. Dorie MJ, Brown JM. Tumor-specific, schedule-dependent interaction between tirapazamine (SR 4233) and cisplatin. *Cancer Res.* 1993;53:4633–4636.
226. Rischin D, Hicks RJ, Fisher R, et al. Prognostic significance of [^{18}F]-misonidazole positron emission tomography-detected tumor hypoxia in patients with advanced head and neck cancer randomly assigned to chemoradiation with or without tirapazamine: a substudy of Trans-Tasman Radiation Oncology Group Study 98.02. *J Clin Oncol.* 2006;24:2098–2104.
227. Patterson AV, Ferry DM, Edmunds SJ, et al. Mechanism of action and preclinical antitumor activity of the novel hypoxia-activated DNA cross-linking agent PR-104. *Clin Cancer Res.* 2007;13:3922–3932.

JNM The Journal of NUCLEAR MEDICINE

Molecular Imaging of Hypoxia

Kenneth A. Krohn, Jeanne M. Link and Ralph P. Mason

J Nucl Med. 2008;49:129S-148S.
Doi: 10.2967/jnumed.107.045914

The Journal of Nuclear Medicine is published monthly.
SNMMI | Society of Nuclear Medicine and Molecular Imaging
1850 Samuel Morse Drive, Reston, VA 20190.
(Print ISSN: 0161-5505, Online ISSN: 2159-662X)

SNMMI SOCIETY OF NUCLEAR MEDICINE AND MOLECULAR IMAGING